Journal of Climate and Community Development
A Double-Blind, Peer-Reviewed, HEC recognized Y-category Research Journal
E-ISSN: 3006-7855 P-ISSN: 3006-7847

Reservoir Characterization of Sawan Gas Field using Seismic Inversion and Machine Learning Algorithms, Central Indus Basin, Pakistan

Hafiz Muhammad Taqi[1] Abdul Basit[2]

[1] MS Geophysics, Petrolead (Seismic Data Management, Oil & Gas Sector), Muscat, Oman.

[2] MS Scholar Geophysics, Bahria University, Islamabad, Campus, Pakistan.

Corresponding Author: Hafiz Muhammad Taqi, **Correspondence through:** hafizmuhammadtaqi@gmail.com

Vol. *5,* ***Issue*** *2, 2026*

Article Information

Received:
2026-05-27

Revised:
2026-07-21

Accepted:
2026-08-09

ABSTRACT

The study's primary goal is to identify the thin sands packages of B and C Intervals of Lower Goru Formation of Sawan Gas Field, by using machine learning along with reservoir characterization by performing seismic interpretation, seismic inversion, petrophysics, Rock physics modelling and using machine learning algorithms. The Sawan Gas Field is situated within the Central Indus Basin of Pakistan, and its geological setting is characterized by extensional tectonic processes. Following the completion of seismic interpretation, seismic inversion, and petrophysical analysis, the findings indicate that the C Interval of the Lower Goru Formation within the Sawan Gas Field exhibits a more substantial hydrocarbon potential when contrasted with the B-Interval. Rock physics modeling have used for the prediction of P and S waves variations and how Poisson's ratio occurs. Rock physics depicted the missing log prediction like S-wave specifically and fluid substitution also occurred with different conditions to confirm reservoir availability. Model Based Inversion (MBI) have been used to predict and confirm better results came from seismic interpretation. Wavelet was extracted from the control line and the correlation occurred. LFM (Low Frequency Models) have been generated as well. Afterwards Quality control of data was occurred by inverted techniques. Lastly to confirm results with seismic inversion technique, Machine learning (PNN) based on Bayesian classifier method which gives reliable prediction of petro physical properties, so it is used predict Volume of clay prediction, Porosity prediction and Saturation of water was predicted by Actual and Predicted values.

Keywords: *Seismic Interpretation, Rock Physics, Lower Goru Formation, Model Based Inversion, Reservoir Characterization.*

Citation: APA
Taqi, H, M & Basit, A (2026). Reservoir characterization of sawan gas field using seismic inversion and machine learning algorithms, central indus basin, Pakistan, Journal of Climate and Community Development, 5(2), 76-114.

Introduction

1.1.Overview

Geophysical methods play a crucial role in exploring subsurface reserves of hydrocarbons and minerals. These techniques involve the examination of distant areas of the Earth through physical measurements, typically conducted on the surface. Additionally, they encompass the interpretation of these measurements to understand subsurface structures and phenomena. The Geophysical technique closely resembles remote sensing, as it involves collecting subsurface information through measurements taken from the surface. Geoscientists employ various methods for exploration, including magnetic, gravity, resistivity, among others. Among these, the seismic reflection method stands out as a widely utilized and efficient tool, contributing significantly to addressing the economic challenges faced by the country. Earth investigation by geophysical method requires taking measurements to inspect the variation both horizontally and vertically through calculating its physical properties (Bust et al., 2010). Seismic interpretation is carried out to comprehensively determine and map the reservoir's location, trapping mechanism, and conduct seal analysis in the study area more. Additionally, inversion allows for the assessment of uncertainties and risks (Pendrel, 2000). Various inversion algorithms play a significant role in providing a valuable link in reservoir management and development (Pendrel, 2000).

1.2.Location Map

The research area is situated within the Thar Desert, Khairpur district, Sindh, with geographical coordinates ranging from 27°17'14.424" N to 26°55'34.3452" N and 69°18' 44.0676" E to 69°18' 40.464" E. The Sawan field is subdivided into three parts – South, Centre, and North – by two major strike-slip faults, as noted by Rahman and Ibrahim in 2009. Geologically, this area is positioned on the Southeastern flank of the North-South trending Jacobabad-Khairpur High. In the Middle Indus Basin, the Sawan delta complex forms a platform slope.

Figure 1.1: *Location Map of Sawan field (after Berger et al., 2009).*

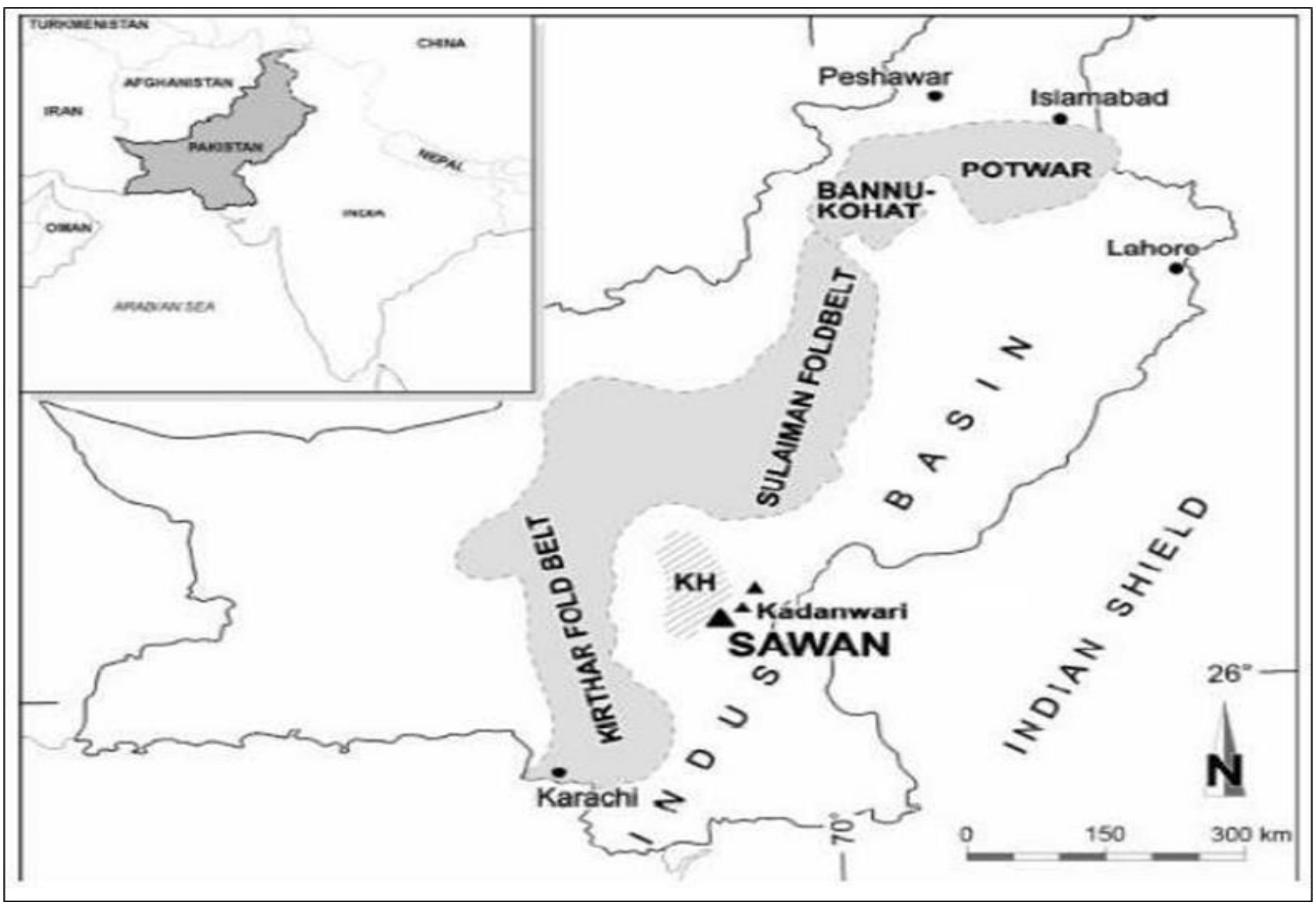

Early Cretaceous Lower Goru "C" Interval Sand formation act as a Prolific, which trapped by distally up dip stratigraphy in westward direction along with some Structural features. The charging source of Lower Goru formation is Sembar Formation of Cretaceous age that was confirmed as regional source having rich organic shale in Lower and Middle Indus Basin (Ahmad et al., 2004).

1.3.Exploration History

The Sawan field, a significant gas reservoir located in the Lower Indus Basin, Khairpur District, Southern Pakistan (Late Cretaceous), spans the geographical coordinates between 24° and 28°N Latitude and from 66°E Longitude to the Eastern boundary of Pakistan. Discovered in 1998 by OMV (Pakistan) Exploration, the Lower Goru Formation sediments were identified by OMV (Pakistan), OGDCL (Oil and Gas Development Company Limited), and various other companies. The Southern compartment houses the accessible PSTM 3D seismic cube covering approximately 10^2 km. Within the Sawan field, 15 wells have been drilled, with the central compartments being the primary producing zone, known as the main gas tank (Ibrahim, 2007). Fourteen of these wells contribute 270 million cubic feet/day to Sui Southern Gas Company, marking it as one of the major gas reserves discoveries in Pakistan with a total proven gas reserve of (2-2.5 TCF).

The primary objective of this study is to map the productive sands of the Lower Goru Formation within the Sawan field.

1.4.Data Set:

The study area, the following data sets (seismic and well) have been used for research work; that is acquired by Land Mark Resources (LMKR) by the permission of Directorate General of Petroleum Concessions (DGPC).

- Customized 3D Seismic Data Cube (10*10 km^2).
- Digital Well Logs (LAS files of three wells).
- Navigation Files.
- Seismic Header Files.
- Formation Tops.

1.4.1. Seismic Data:

The OMV-Sawan-3D-1999, Seismic Block (10*10 km^2) that has been used for studying the area, marking horizons and identification of stratigraphic or structural geometries. The 3D Seismic Data Cube is formed of In-Lines and Cross Lines. The In-Lines ranges from 718 to 858. The Cross Lines ranges from 874 to 1004.

1.4.2. Well Data:

Three Wells (Sawan-01, Sawan-07 & Sawan-08), have been used for research purposes in Sawan area. Sawan-01 is used to generate Synthetic Seismogram and for well to seismic tie.

Table 1.1: *Well Data Used in Reservoir Characterization.*

Well Name	Latitude	Longitude	Status	Class	TD(m)
Sawan-01	26.991828	68.906992	GAS	Exploratory	3587
Sawan-07	26.999283	68.923317	GAS	Development	3400
Sawan-08	27.009156	68.933394	GAS	Development	3430

1.5 Software Used

- Petrel Software
- Geographix Software
- HRS software

1.6 Literature Review

One of the widely used methods for characterization of the reservoir is seismic inversion. Seismic inversion aids in combining the seismic and well data for predicting the characteristics of reservoir (Wang et al., 2017). Reservoir characterization of mixed facies and tight sands in Central Indus Basin Pakistan was performed by (Toqeer et al., 2021). By making use of seismic data and well log data as an input reservoir modeling, model based seismic inversion and post stack seismic inversion was done along with generation of cross plots of effective porosity and acoustic impedance. By making use of seismic attributes interpreters are able to extract more information from original seismic data. By using 2D seismic data as input and by performing seismic attribute analysis, Goru Clastic of Indus Basin Pakistan were evaluated by (Tayyab et al., 2017).

Artificial neural network and seismic inversion analysis were used (Qiang et al., 2020) to predict the reservoir quality of Sawan Gas field, Pakistan. During this research cross plots of porosity and acoustic impedance were created and support vector machine was used (Qiang et al., 2020).

1.5.Purpose of Research

So, our research will focus on thin bed detection by seismic attributes. Cross plot porosity and permeability prediction by making use of Machine Learning and neural network, computation, and validation of shear sonic using machine learning, geomechanical parameters calculation, and creation of cross plots such as Vp, Vs, density etc.

1.6.Base Map:

The Base Map serves as the fundamental representation of primary data, illustrating the orientation of 3D In-Line and Crosslines, and indicating the position of wells with Projected Coordinates (X, Y). In this visualization, In-Lines are oriented from the Northwest (N-W) to the Southeast (S-E), while Crosslines are directed from the Northeast (N-E) to the Southwest (S-W). The accompanying figure showcases the 3D Survey of the Sawan Gas Field, specifically utilized for research purposes.

Figure 1.2: *Base map of Sawan Gas Field.*

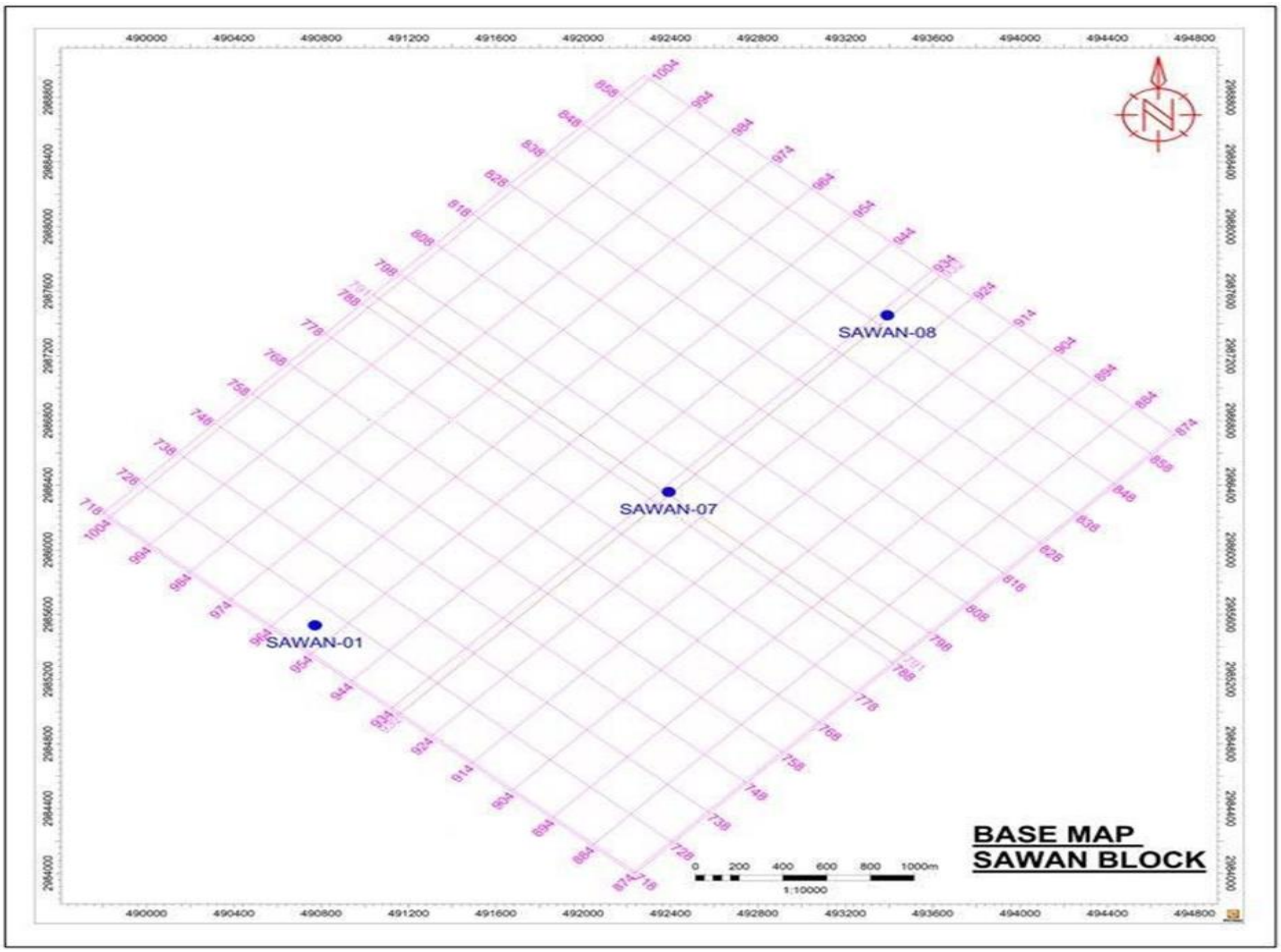

1.7. Objectives of the Study:

The main objective of the research is to better evaluation of C-Interval Sand of Lower Goru formation with the help of different quantitative approaches.

- Analyzing detailed 3D seismic interpretation to find out subsurface structures favorable for hydrocarbon accumulation.

- Examining rock properties and fluid content for essential reservoir insights using petrophysical analysis.
- Characterizing reservoir properties on a larger scale using inversion techniques.
- Utilizing machine learning techniques for the estimation of petrophysical parameters in reservoir formations.
- Using rock physics models for the evaluation of low-impedance sand packages.

1.8.Research Methodology

The research commenced with a comprehensive review of the geological and tectonic aspects of the study area. One-dimensional (1D) forward modeling, specifically synthetic seismogram generation using seismic and well data, was employed to establish optimal correlation between synthetic and actual seismic data at well locations, accurately marking horizon positions. Subsurface geometry was then depicted through two-dimensional time and depth contour maps using Kingdom 8.6 Software.

Petrophysical analysis utilized high-resolution well log data, displaying logs such as Spontaneous Potential (SP), Gamma Ray (GR), Caliper Log (CALI), Deep Laterolog, Shallow Laterolog, and Micro Spherical focused log. Porosity tracks incorporated Sonic log (DT), Density log (RHOB), Neutron log (NPHI), enabling the determination of Shale Volume (Vsh) and various porosity measures like Density Porosity (DPHI), Total Porosity (PHIT), and Effective Porosity (PHIE), along with water and hydrocarbon saturation.

Figure 1.3: *Methodology workflow adopted for the execution of this dissertation.*

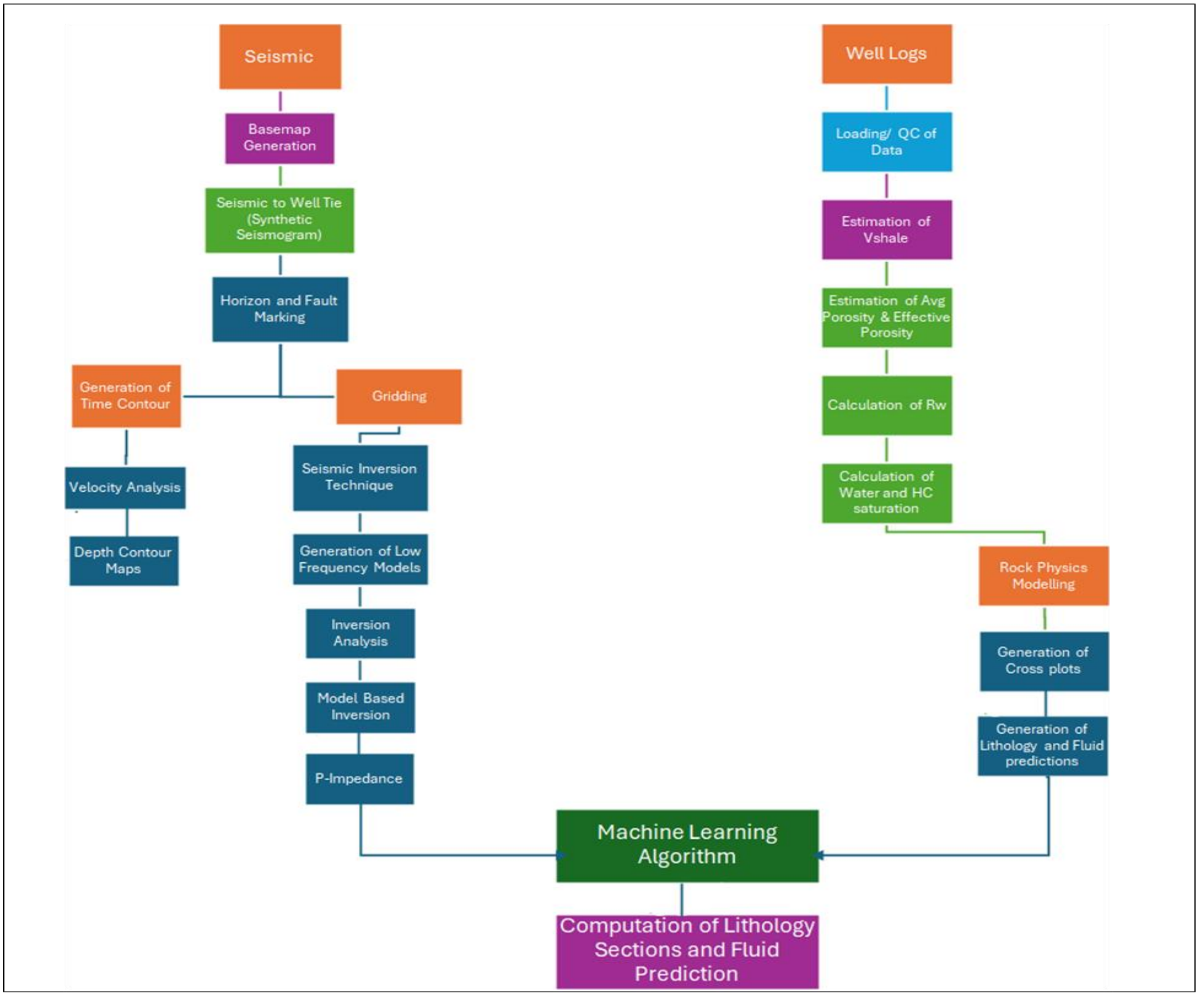

Geology of Study Area

2.1. Introduction

The geology of the study area is a crucial factor in seismic and stratigraphic interpretation, as highlighted by Bacon et al. (2003). Geophysicists need a profound understanding of both local and regional geology for accurate seismic interpretation, as emphasized by Badley (1987). Geology describes origin, mode of deformation, structural style, and depositional environment. Therefore, the interpreter must have the knowledge of geology of the study area to overcome the complexities during interpretation.

2.2. Geological Settings

Based on structural development, stratigraphic style, and sedimentary history, the Indus Basin is categorized into three major parts:

- Upper Indus Basin
- Central Indus Basin
- Lower Indus Basin

Moreover, Jacobabad, Khairpur, and Mari Khandkot are identified as elevated areas within the Indus Basin, located in the central and southern parts. Historically, these high areas have played a significant role in the discovery of major hydrocarbon deposits, providing effective trapping mechanisms through their structural and stratigraphic styles. Combined traps, conducive to migration pathways, reservoir charge timing, and hydrocarbon accumulation, have been identified as particularly favorable (Kazmi and Jan, 1997).

Figure 2.1: *Geological Map showing Sawan Area (Ashraf et al., 2021).*

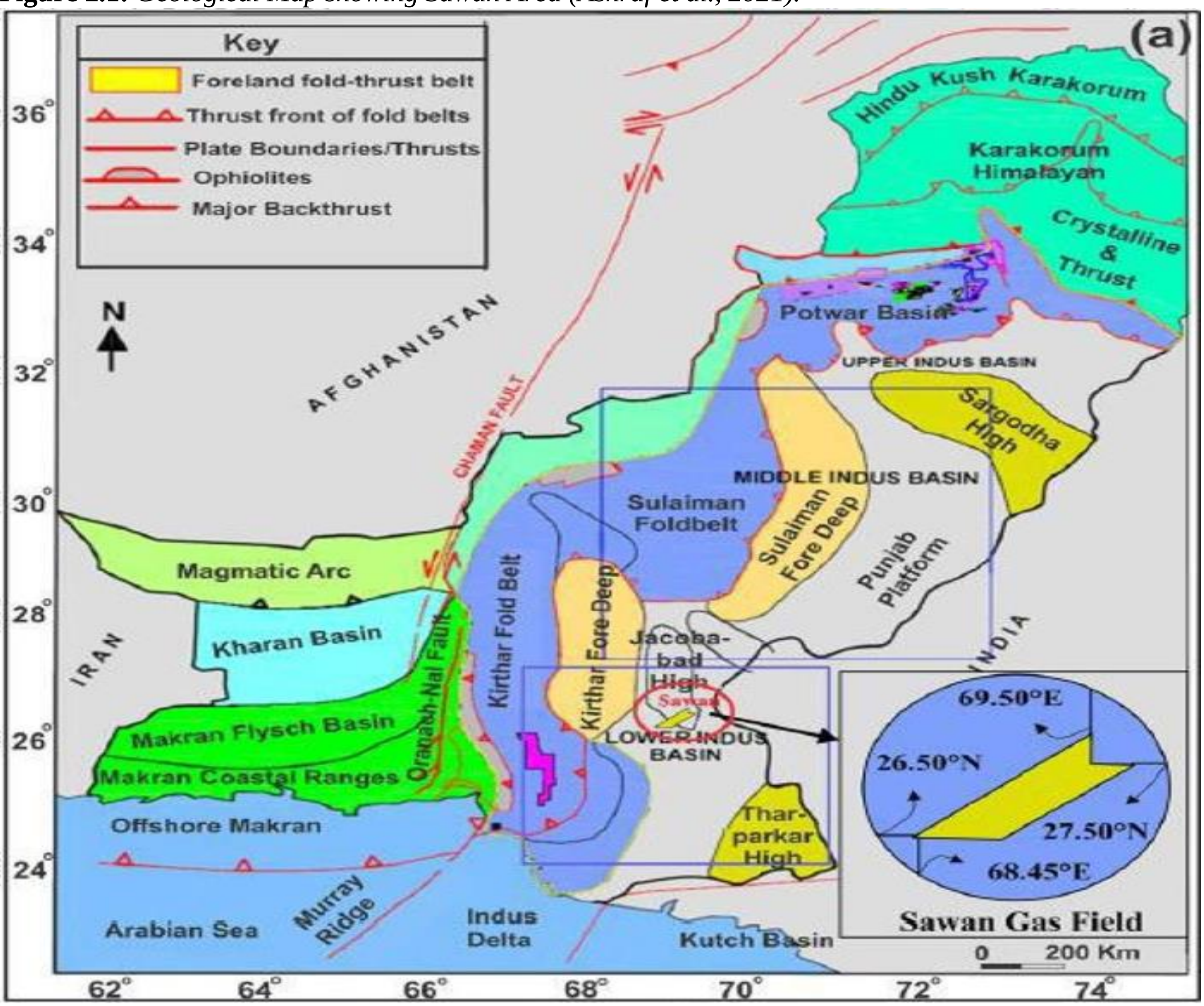

2.3. Tectonic Settings

The unveiling of the Lower Goru primarily occurred on the Jacobabad High and Mari High within the Lower and Central Indus Basin, known for their structural characteristics. These structural highs serve as migration pathways and are conducive to hydrocarbon accumulation. Three tectonic episodes associated with post-rifting have shaped the structural configuration. (Ahmad et al., 2004).

The initial episode is the Cretaceous uplifting and deterioration occurred near the K-T boundary, marked by Late Cretaceous Uplifting. The reduction of Ranikot clastic rocks around the Paleo high and their subsequent increase confirmed this event. The second episode resulted from the collision of the Indian and Eurasian plates. The Indian plate's anti-clockwise rotation led to wrench faulting, particularly impactful to the east of the Sawan area. (Ahmad et al., 2004).

Figure 2.2: *Tectonic Map of Lower Indus Basin (Rehman et al,2013)*

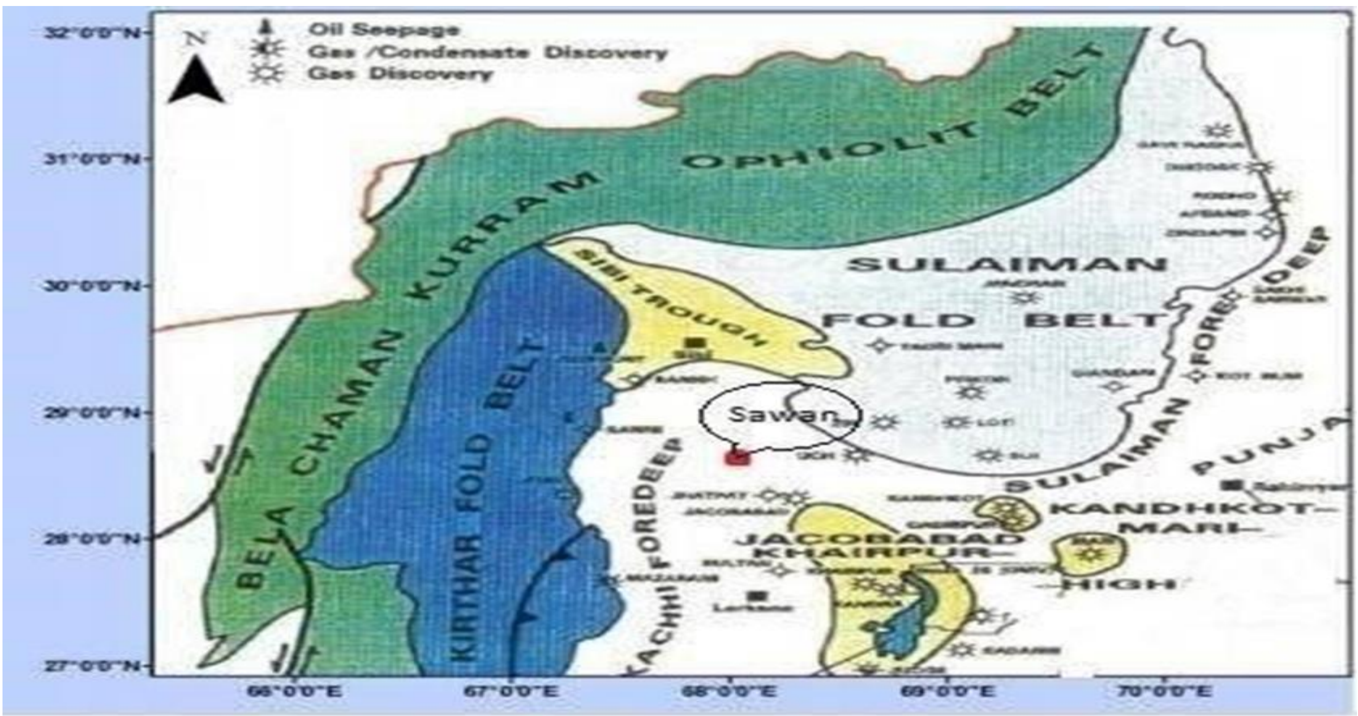

The figure illustrates significant discoveries in the Lower Indus Basin, including the location of the study area, such as the Sawan Gas Field. Situated in the Southern Indus Basin of Pakistan, Sawan Gas Field spans between 24° and 28°N latitude and from 66°E longitude to the eastern boundary of Pakistan (Zaigham and Mallick, 2000).

2.4. Stratigraphy of Lower Indus Basin

The stratigraphic sequence in the Sawan area exhibits variation from East to West. Pre-Cambrian basement rocks are prominent in the southeastern portion of the basin, while towards the West, the sedimentary sequence thickens. The Jacobabad–Khairpur high encompasses Tertiary, Mesozoic, and Quaternary lithologies, with a key unconformity occurring between the base Permian and base Tertiary, indicating deposition during the early rifting stage. The Goru Formation, lithologically divided into Lower Goru and Upper Goru, is a focus in this study, particularly the Lower Goru.

Table 2.1: *Generalized Stratigraphy of the Lower Indus Basin (Kadri, 1995)*

AGE	FORMATION			LITHOLOGY	SYMBOL	PLAY SYSTEM
PLEISTOCENE	SIWALIK			SANDSTONE & CLASTIC CLAY		
EOCENE	KIRTHAR			SHALE & MARL		
	LAKI			LIMESTONE & SANDSTONE		
PALEOCENE	RANIKOT			LIMESTONE & SANDSTONE		
	KHADRO			SANDSTONE, SHALE & LIMESTONE		
CRETACEOUS	PAB			SANDSTONE		
	MUGHAL KOT			MUDSTONE & SHALE		
	PARH			LIMESTONE,SHALE & MARL		
	UPPER GORU			LIMESTONE & SHALE		SEAL ROCKS
				UPPER GORU SHALE		
	LOWER GORU	UPPER SAND		A SAND		RESEVOIR ROCKS
				TURK SHALE		
				B SAND		
				BADIN SHALE		
				C SAND		
				JHOL SHALE		
				D SAND		
				UPPER SHALE		
		MIDDLE SAND		MIDDLE SAND		
				LOWER SHALE		
		BASAL SAND		UPPER BASAL SAND		
				TALHAR SHALE		
				LOWER BASAL SAND		
	SEMBAR			SEMBAR SAND & BLACK SHALE		SOURCE ROCKS
JURASSIC	CHILTAN			LIMESTONE & SANDSTONE		

2.1. Petroleum Play

In the petroleum system of the Sawan area, the source, reservoir, and cap/seal rocks, with the migration of hydrocarbons playing a pivotal role. The drilling and logging results indicate the presence of a complete petroleum system of Cretaceous age in the Sawan area.

- Sembar Formation
- Goru Formation
- Chiltan Formation.

2.5.1. Source Rock:

Based on previous study, it has been considered that Sembar Formation and Goru Formation serve as the major source rocks in the Central and Lower Indus Basin. In the Western part of the Southern Indus Basin, secondary source strata consist of transgressive marine shales of Upper Paleocene age, which are buried (Zaigham and Mallick, 2000).

2.5.2. Reservoir Rock:

The Lower Goru Formation, a key reservoir rock in the Sawan field, is characterized by intercalations of sand-shale layers. Within the lower portion of the Cretaceous Goru Formation, there are high-quality reservoir sandstones, categorized as A, B, C, and D.

In the Lower Indus Basin, multiple sealing intervals, including the substantial Ghazij Shales, Lower Goru Shale intervals, and the Ranikot Shale unit, are present (Shah, 2009). The thick shale bed of the Upper Goru from the Late Cretaceous acts as a seal for C-Sands reserves in the Lower Indus Basin. Structural-cum-stratigraphic traps have been identified in the Sawan area, developed during the third phase of tectonic events known as the inversion.

Seismic Data Interpretation

Seismic interpretation's primary goal is to precisely characterize the lithology and subterranean geological formations. Rocks that contain hydrocarbons can be distinguished from rocks that do not by using seismic data analysis (Ahmad et al., 2021). Seismic interpretation becomes quite challenging in areas of complex tectonics. Therefore, in such cases in order to carry out accurate interpretation it is necessary to make correct observations in both subsurface as well as surface data (Zamora et al., 2022).

To perform Seismic Interpretation, the following workflow is adopted.

3.1 Seismic Interpretation's Workflow

Figure 3.1: *Workflow adopted for seismic interpretation adopted during research.*

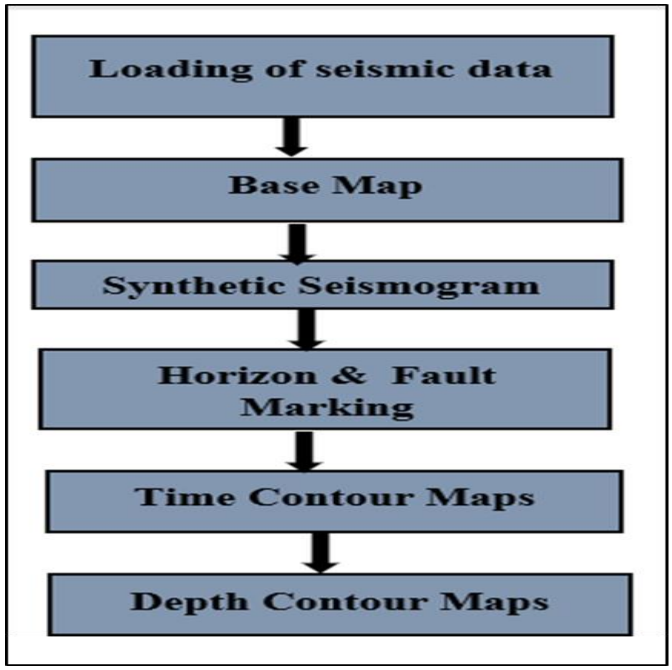

3.1.1 Loading of Seismic Data

A 3D seismic data cube in SEGY format of Sawan Gas Field area was provided by DGPC. The data was loaded into Petrel software by using the SEG Y headers for cross line and inline loading.

3.1.2 Base Map

After the completion of the seismic data loading, the base map of the provided cube is generated. The base map displays how the overall grid is oriented. There are two types of lines in a 3D cube: in lines and cross lines. The cross line lies between the numbers 390 and 540, as illustrated in Figure 3.2, while the inline runs from 1310 to 1470. The Sawan-01 is located on inline 1459 and cross line 520, Sawan-07 is located on inline 1407 and crossline 420.

Figure 3.2: *Base map of the study area showing the distribution of in lines and crossline along with type of well.*

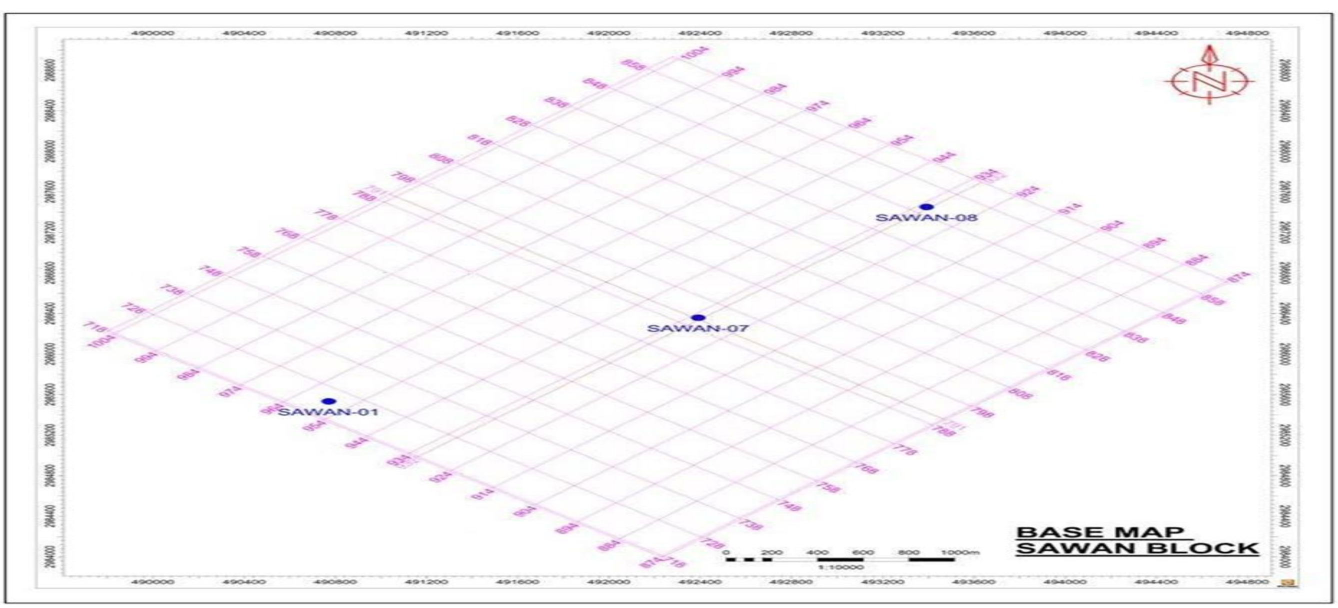

3.1.3 Synthetic Seismogram

Synthetic seismogram serves as a "tie" in hydrocarbon exploration between seismic reflection data collected at the same location and changes in rock characteristics observed in a borehole (Helmberger et al., 1989). The wavelet derived from seismic data is convolved with the reflectivity derived from digitized acoustic and density logs to generate the synthetic seismogram. Interpretations of data can be improved by comparing the marker beds or other correlation points noted on the well logs with the notable reflections on the seismic section (Helmberger et al., 1989).

A seismogram is necessary for a well-to-seismic tie. Therefore, density log and sonic log from the Sawan 01, Sawan 07 and Sawan 08 along with gamma ray log is also used as a references log.

Figure 3.3: *Synthetic Seismogram of Sawan-07*

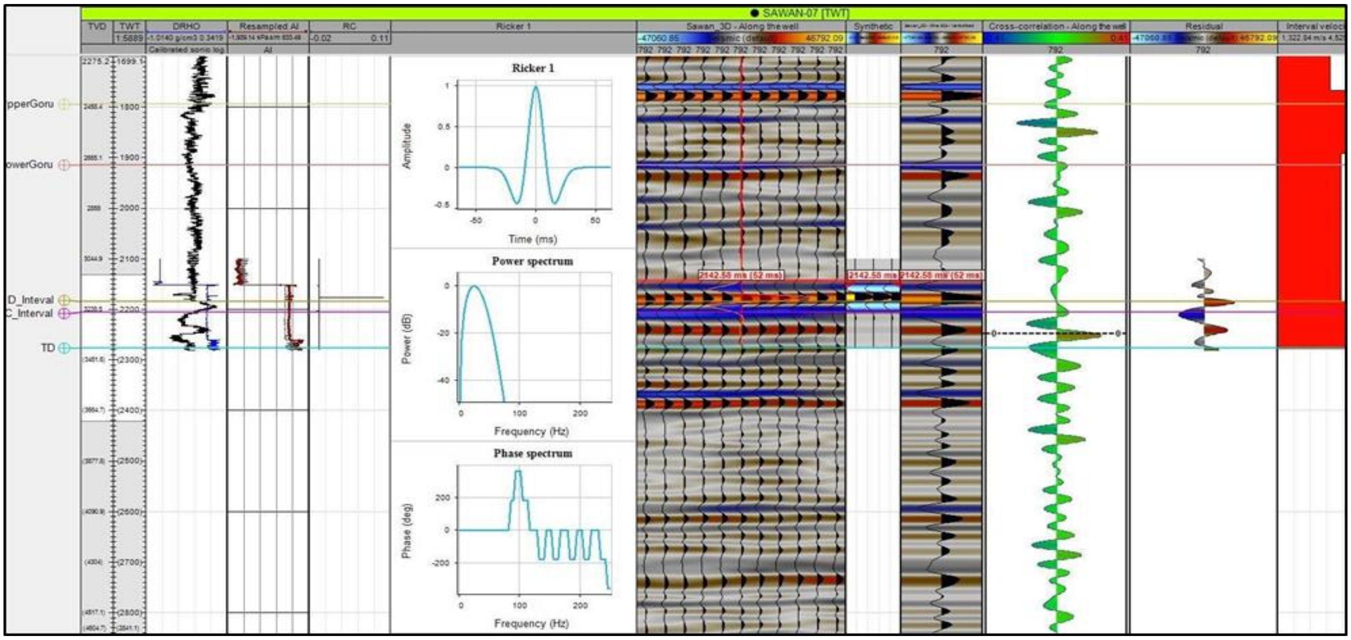

3.1.4 Horizon and Fault Marking

Interpreting and marking various horizons on seismic data is the first and most fundamental step in seismic interpretation. Understanding the structure and stratigraphy of the research area is necessary for accurate interpretation. Two horizons are interpreted. namely C-Interval and D-Interval. These are the sand intervals of Lower Goru Formation.).

The research area's fault extension is defined by fault correlation, which also delineates dip directions and specifies the throw which is actually vertical component of the separation and heave which is the horizonal component of slip. The fault correlation aids in defining the fault's network. On seismic data the faults are interpreted when there appears a certain breakage on the seismic section (Freeman et al., 1991).

Interpreted Sections:

On the seismic section two horizons C-interval and B-interval were marked both lie within 2 to 5 seconds.

Figure 3.4: *Seismic section of Inline-724 with well location of Sawan- 01 along with the Upper Goru formation and C and B Intervals.*

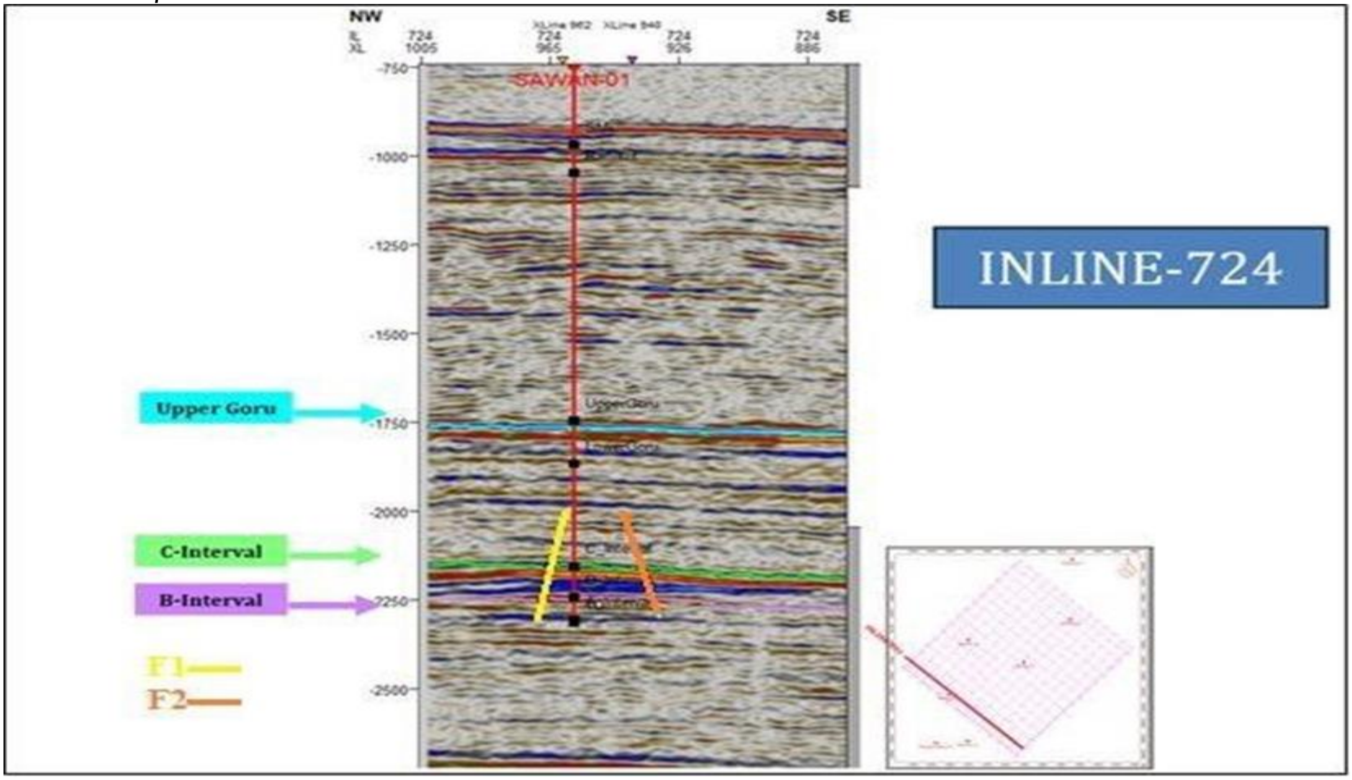

Figure 3.5 *Seismic section of Xline-724 with well location of Sawan- 01, Sawan-07 and Sawan-08 along with the Upper Goru formation and C and B Intervals.*

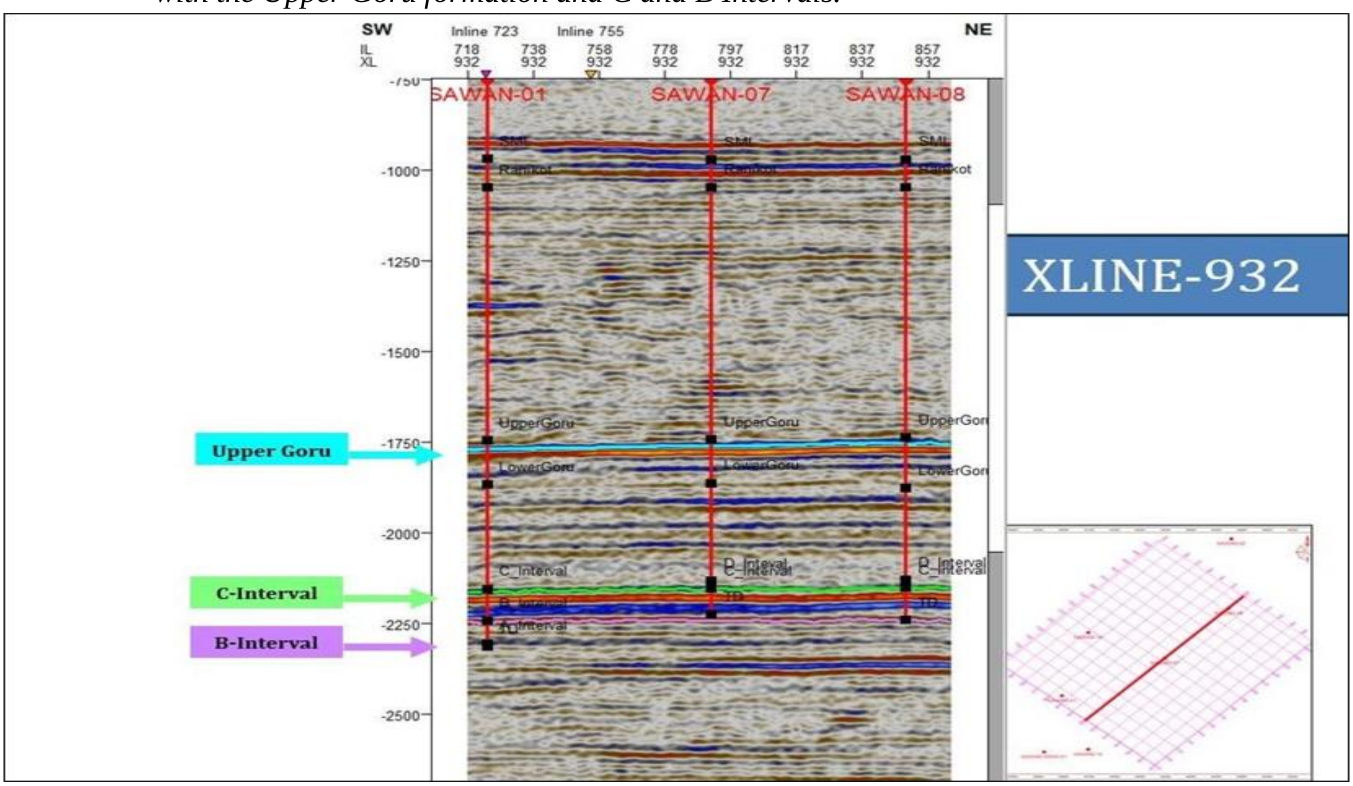

3.1.5 Preparation of Contour Maps

The creation of contour maps is the last stage of interpretation. Lines that connect points of the same depth, height, or time are called contours.

TWT contour maps are initially created in the seismic interpretation, followed by depth contour maps. Seismic maps are another name for contour maps. The seismic map is typically the end result of seismic exploration, the one on which the success of the entire exploration's operation depends. A map may be used to highlight specific areas during meetings with the management, but the map itself is crucial for deciding where and if to drill for oil (Caputo & Postpischl, 2010).

3.1.6 Interpretation of C-interval Maps

Based on seismic data seen in the time and depth maps of the C-interval horizon, two faults designated as F1 and F2, are interpreted in the C-interval horizon. Both mentioned faults are normal faults.

Figure 3.6: *The Time Contour Map of C-Sands formation.*

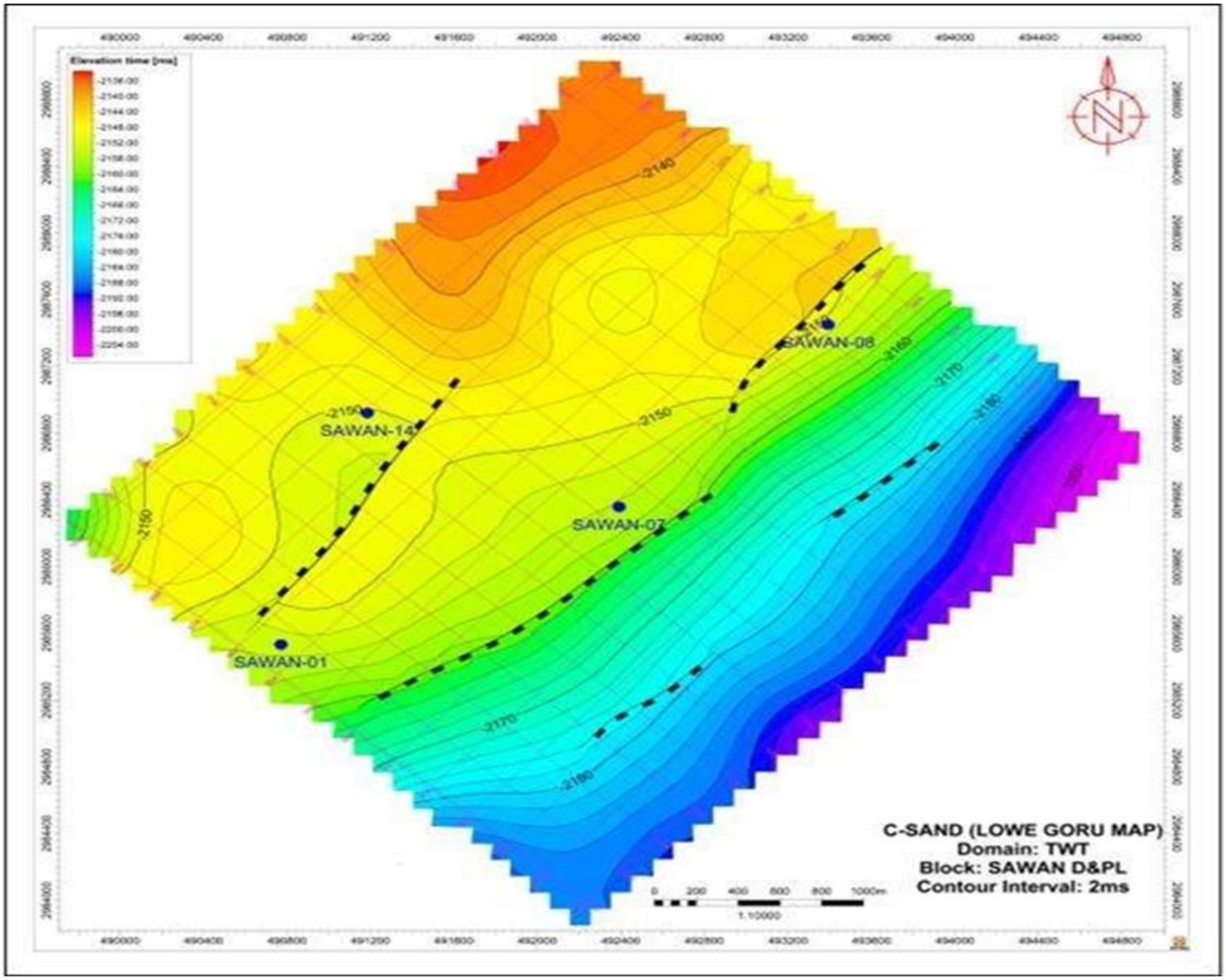

As shown in Figure 3.8 depth contour map of C interval ranges from 3170 to 3260 m. The contour interval in this map is 10 m. The unit of the depth contour map is meters.

Figure 3.7: *Depth Contour map of C-Sands.*

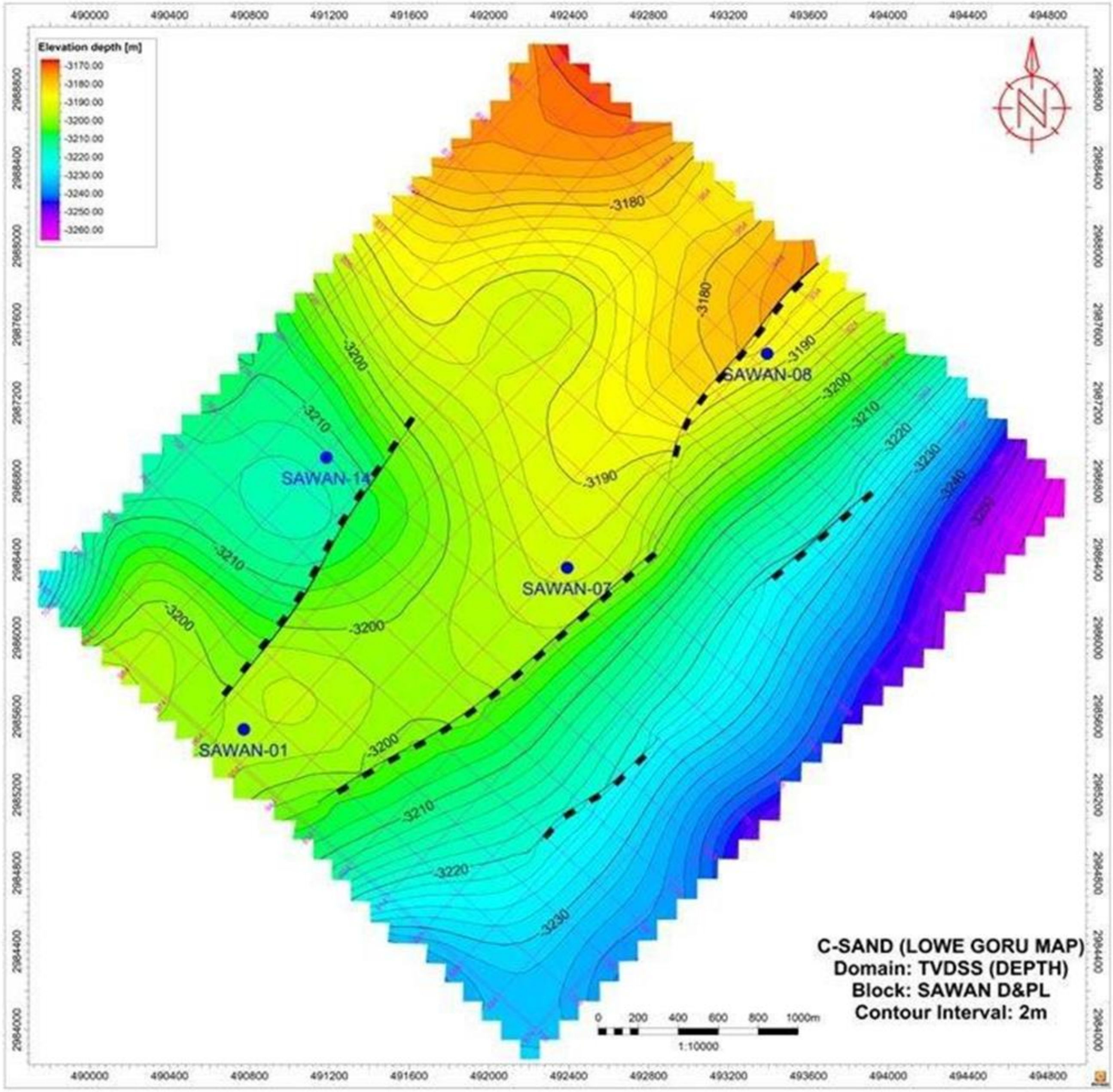

3.1.7 Interpretation of B-interval Maps

The time contour map of B-interval map ranges from 2228 to 2284 milliseconds. The contour interval is 5 milliseconds. Time contour values are highest at the eastern side of B-interval map depicting that the horizon becomes deeper in the eastern side whereas the time contour values are decreasing towards the west showing that at the western side the horizon becomes shallow.

Figure 3.8: *The Time Contour Map of B-Sands member of Lower Goru.*

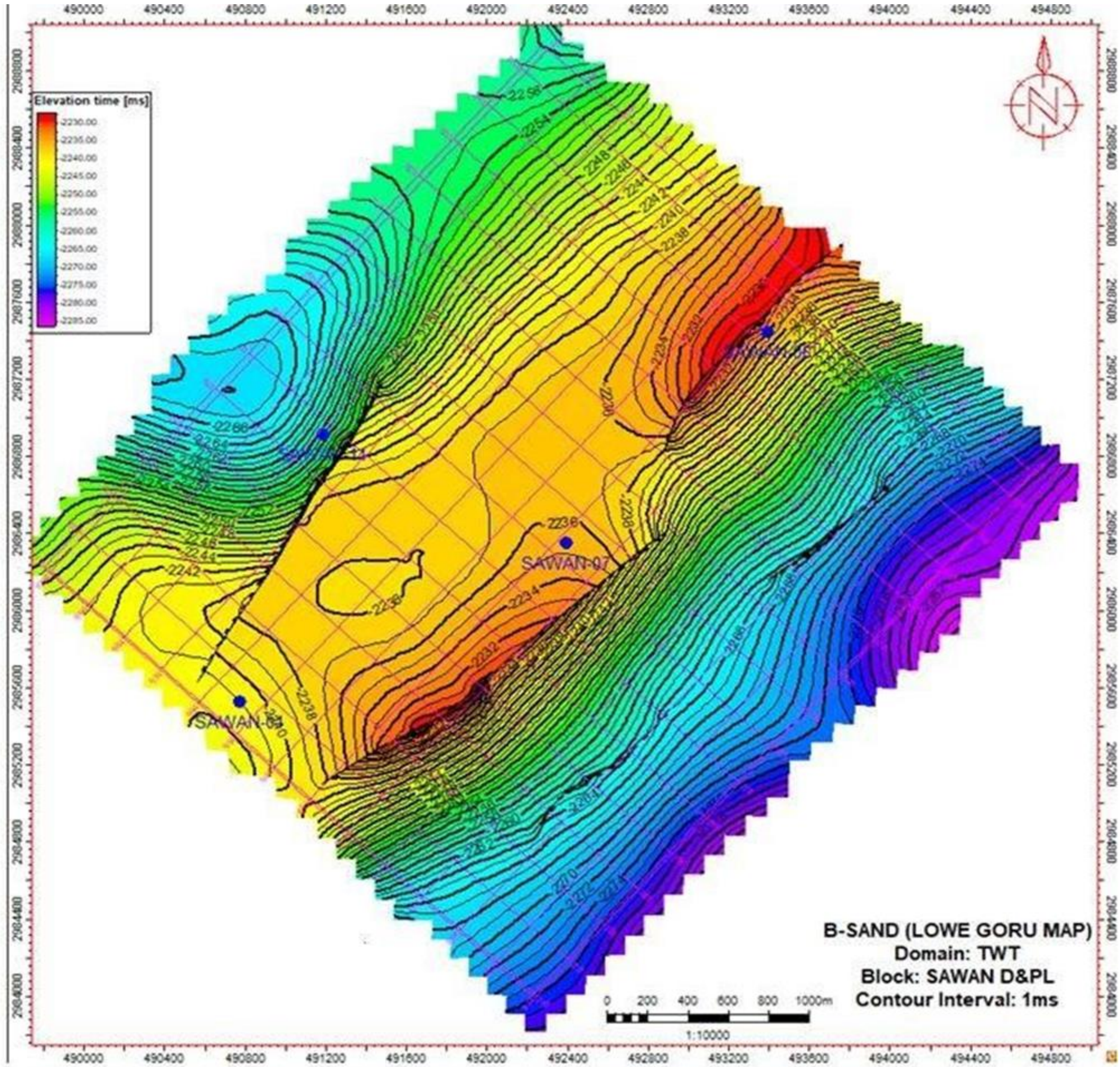

Figure 3.9: *Depth Contour Map of B-Sand that is Member of Lower Goru Formation.*

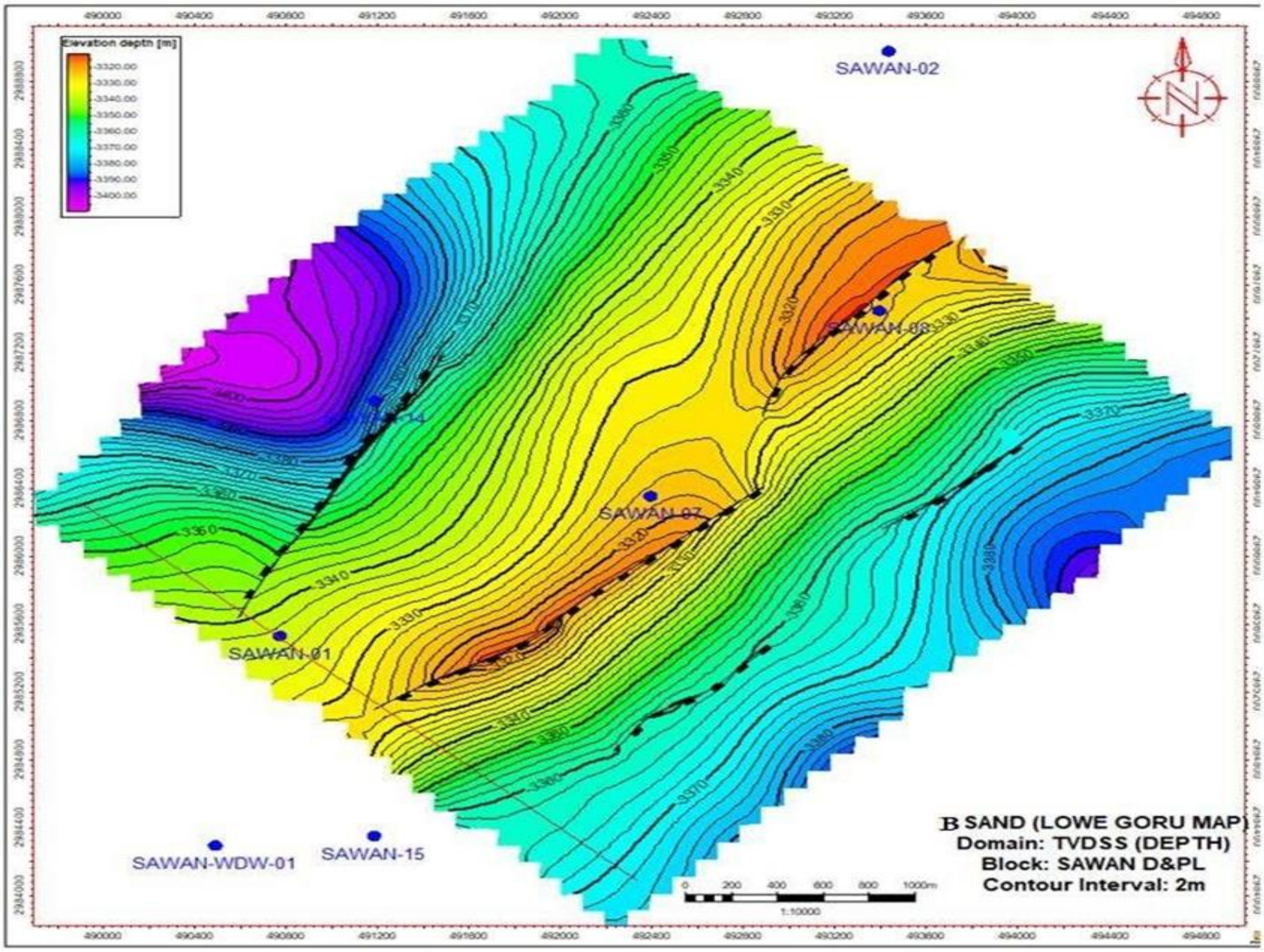

As shown in Figure 3.10 the depth contour map of B-interval ranges from 3320 to 3400 m. The contour interval in this map is 10 m. The unit of depth contour maps is meters.

Petrophysics

4.1 Introduction

Petrophysics is the study of the physical properties of subsurface rocks and their interactions with fluids, encompassing gases, liquid hydrocarbons, and aqueous solutions (Donaldson and Tiab, 2004). This discipline enables the identification of fluid properties within a reservoir and the creation of a geological profile within a borehole (Ali et al., 2014).

4.2 Petrophysical Analysis

The Petrophysical analysis has been carried out for the reservoir characterization of the Sawan field. Well logs data of Sawan-01 and Sawan-07 has been utilized to evaluate the different formations.

Steps adopted to perform petrophysical analysis:

- LAS files loading.
- Marking Zone of Interest
- Calculation of Vsh and Vclean
- Porosity Estimation
- Calculation of Rw
- Water Saturation
- Hydrocarbon Saturation

4.3 Lithology Identification

Lithology identification involves the use of Gamma-Ray (GR) logs, SP logs, and Caliper logs, with the Gamma-Ray log being a crucial indicator. The GR log measures and identifies the radioactivity within rock formations, primarily arising from the presence of radioactive minerals like Uranium, Potassium, and Thorium. This log is instrumental in distinguishing between shale and clean formations such as sand (Rider, 2012).

In the linear method, the Index Gamma Ray (IGR) is computed, representing Vsh (volume of shale):

$$\text{Volume of shale} = \frac{(GR)log-(GR)min}{(GR)max-(GR)min}$$

Where,

GR_{log} = Formation's radioactive values

GR_{max} = Maximum value of gamma ray

GR_{min} = Minimum value of gamma ray

Index Gamma Ray (IGR), give us maximum volume of shale, and we must find minimum volume of shale by non-linear method.

Non-Linear Method:

In the non-linear method, various formulas, including Stabier, Larinov, and Clavier, are employed to calculate the minimum volume of shale. Among these formulas, Stabier is often chosen as it provides the minimum volume of shale.

- **Stabier:** (Most preferable)

$$Vsh = \frac{IGR}{3-2\,IGR},$$

where, IGR= Index Gamma Ray, Vsh is Volume of Shale

- **Larinov:** (Used for Older rocks)

$$Vsh=0.33(2^{2\,IGR}-1)$$

- **Clavier:**

$$Vsh=1.7-(3.38-(IGR+0.7)^2)^{0.5}$$

Volume of Shale (Vsh) can also be estimate through SP log, Density and Neutron log. Caliper log evaluates the borehole (BH) geometry and identifies a lithology. Different conditions of logs pattern used for lithology discrimination i.e. straight log pattern shows that clean reservoir formation.

4.4 Porosity

Porosity is defined as the ratio of the volume of voids to the total rock volume, representing the measure of empty spaces within a rock (Donaldson, 2015). It is a crucial parameter in reservoir assessment. High porosity values indicate rocks with a greater capacity to hold fluids. The porosity of rocks varies based on factors such as grain size, sorting, and cementation, typically falling within the range of 5% to 50% in reservoir rocks. Total porosity is determined using Sonic, Density, and Neutron logs, either individually or in combination. Effective porosity, crucial for reservoir evaluation, is calculated by accounting for the influence of shale (Mavko et al., 2009).

Next, we have to calculate porosity parameters such as:

- Density porosity
- Sonic porosity
- Effective porosity
- Neutron porosity (Given)

4.4.1 Density Porosity

Density-derived porosity is determined by measuring the bulk density of the formation, where the measuring parameter involves a combination of the rock matrix and fluid (George, 1982; Rider, 1995). The combination of Density and Neutron logs is particularly significant for detecting hydrocarbons, with a crossover between them often indicating the presence of hydrocarbons. The calculation of density-derived porosity is performed using the following equation (George, 1982).

$$\Phi_{\text{density}} = \frac{P_{\text{log}} - P_{\text{Matrix}}}{P_{\text{Fluid}} - P_{\text{Matrix}}}$$

Where,

P_{log} = density of formation.

P_{Matrix} = density of matrix

$P_{\text{Fluid}-}$ = fluid density.

Different matrices densities are as follows:

Sandstone = 2.6 (g/cc)

Fresh mud = 1 (g/cc)

Salt mud = 1.1 (g/cc)

4.4.2 Sonic Porosity

Porosity derived from the sonic log is referred to as Sonic porosity. The sonic log measures the transient time of elastic waves, where the lithology and porosity of the formation contribute to slowness. Sonic porosity logs offer various advantages, including porosity determination, lithology identification, facies recognition, and source rock identification. (Asquith and Gibson, 2004).

$$\varphi_{sonic} = \frac{\Delta T_{\text{log}} - \Delta T_{\text{matrix}}}{\Delta T_{\text{fluid}} - \Delta T_{\text{matrix}}}$$

ΔT_{log} = Transient time of log in formation.

ΔT_{matrix} =Matrix. transient time

ΔT_{fluid} = Fluid Transient time.

Table 4.1: *Different transient time at different matrix is as follow:*

Matrix	Transit Time [ΔT log (microsec/ft)]
Sandstone	55
Mud	189
Salt	185

Hydrocarbon affects the interval transit time or delay time of formation increase. This influence should be removed because it affects the values of calculated porosities, thus their effect can be corrected via following equation: φ= φ□□□□□* 0.7(gas) (Rider, 1995).

4.4.3 Effective Porosity

The interconnected pores or spaces within a rock that facilitate fluid flow or permeability in a reservoir are referred to as effective porosity. Effective porosity excludes isolated pores and water absorbed on clay minerals. The effective porosity log can be created by utilizing total porosity logs and volume of shale logs. Effective porosity is typically less than total porosity. It is calculated by subtracting the shale volume from the total volume of the rock and is determined by the following formula:

$$\Phi_{eff} = \Phi_{avg}*(1-v_{sh})$$

Where

Φ_{avc} = Average porosity

v_{sh} = Shale Volume

(Rider, 1995).

4.4.4 Neutron Porosity

Neutron log that is helpful for measuring hydrogen content within formation and determination of the porosity of formation (George, 1982). i.e., Count Rate will be low in high porosity rock and vice versa. Neutron strikes with nuclei of formation then loss of energy occurs. hydrogen atoms of same mass collide with neutrons; then maximum loss of energy occurs. Thus, Gas bearing Sands show low neutron porosity value due to low concentration of hydrogen ions and Shales shows, high neutron porosity values. Moreover, neutron porosity is given in the data and calculated by well log w.r.t depth (Donaldson, 2015).

4.4.5 Saturation of Water

The quantity of pores volume that filled up with formation water is known as water saturation and water saturation can be calculated by having resistivity of water (Rw). Different models that are used for water saturation i.e. Archie's equation, Indonesian and Dual-Water-Based on the lithology. For Clean Sand, Archie's eq. gives an accurate result. Indonesian eq. is used for the calculation of water saturation

Sw= sqrt(1/RT) / (Vsh^(1- 0.5*Vsh) /sqrt(Rshl) + sqrt(PHIE^m / (a*Rw)))

Where

RT=True resistivity of formtion

Vsh= Shale Volume.

Rshl=Resistivity of shale.

PHIE=Effective porosity.

Rw=water resistivity value.

m=Cementation factor.

a=Turosity factor.

Rw is important for water saturation. It can be calculated by having various parameters such as bottom-hole temperature, surface temperature, water salinity in ppm and SP (static. There are two methods that has been utilized for Rw: Pickett Cross plot method and SP method) (Amigun et al., 2012).

Figure 4.1: *Resistivity of water for Sawan 01 by Pickett plot method.*

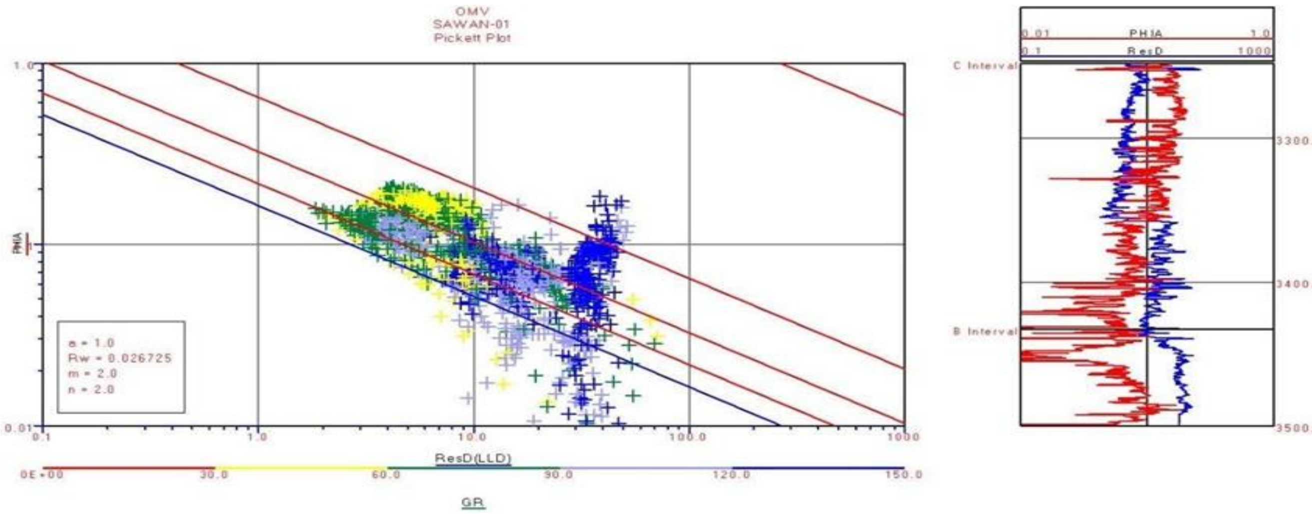

Figure 4.2: *Resistivity of water for Sawan 07 by Pickett plot method.*

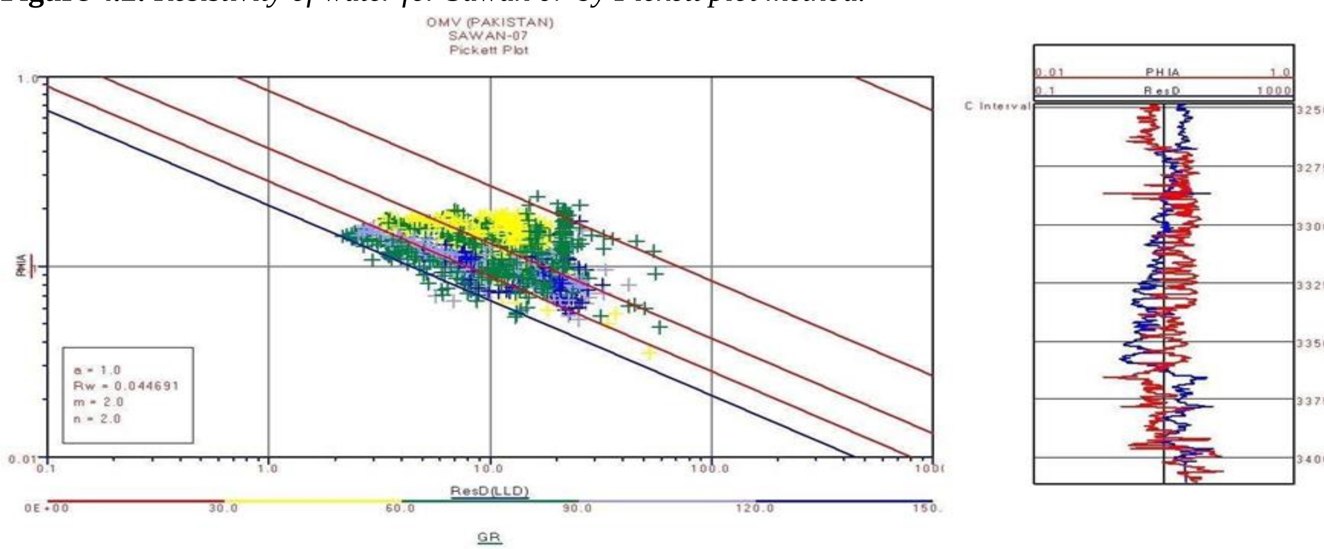

4.4.6 Calculation of Archie Water Saturation (Sw)

The amount of water in a formation is known as water saturation (Ahmed, 2009). Archie's equation provides a mathematical method for calculating water saturation, and resistivity logs are employed for this purpose. The water saturation of the reservoir zone can be calculated using the following formula:

$$S_w = \left\{\left(\frac{a * R_w}{R_t * \varphi A^m}\right)\right\}^{\frac{1}{n}}$$

Where,

- S_w = water saturation,
- φA = average porosity,
- a= lithological coefficient (taken as 1),
- m= cementation factor (taken as 2),
- n= saturation exponent (taken as 2).
- R_t = True Resistivity
- R_w = Water Resistivity

4.4.7 Calculation of Hydrocarbon Saturation (Sh)

Water saturation (Sw) is the percentage of pore spaces that contain water, while hydrocarbon saturation (Sh) represents the remaining fraction containing oil or gas. The formula used to calculate hydrocarbon saturation is given by:

$Sh = 1 - S_w$

4.5 Petrophysical Interpretation of B interval

The petrophysical analysis of the B and C intervals of the Lower Goru Formation in the zone of interest was conducted. The process began with loading the LAS files of Sawan 01 and Sawan 07 wells using the Prizm module of the Geographix software. Zones of interest were identified based on the criteria mentioned above. It was observed that, following the specified criteria, two zones were marked in the B interval of Sawan 01 well, and one zone was marked in the B interval of Sawan 07 well. The analysis likely involved assessing the petrophysical properties and characteristics of these marked zones to evaluate their reservoir potential.

4.5.1 Petrophysical Interpretation of B Interval Sawan 01

Figure 4.3: *Petrophysical analysis of Sawan 01 on B-Interval of Lower Goru Formation.*

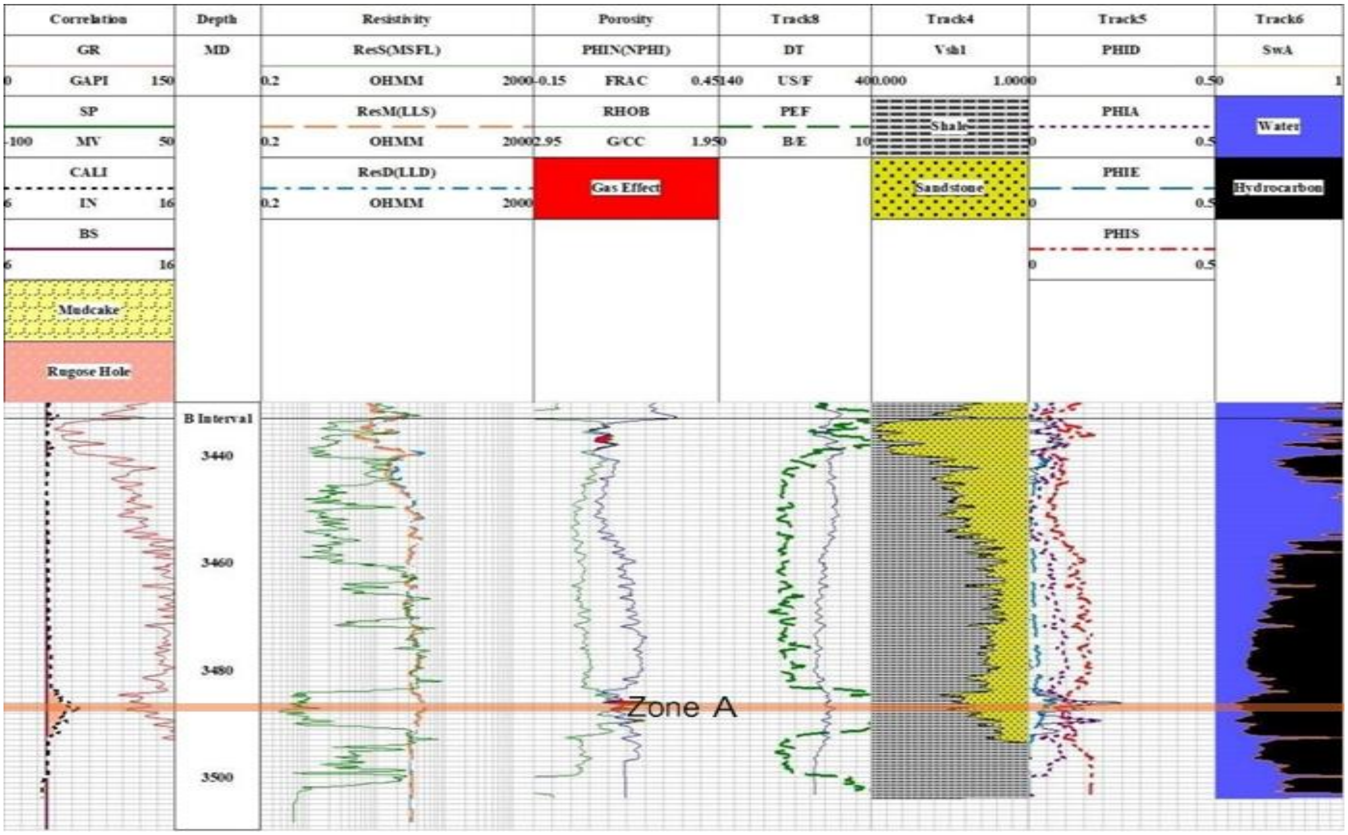

In the Lower Goru B-Interval of Sawan 07 well, a zone of interest was identified. This zone was observed within the depth range of 3486-3487 m, in the interested zone, the gamma ray value was on the lower side, separation between MSFL and LLD was observed. There was presence of gas effect i.e., neutron and density crossover were observed. And lastly the hydrocarbon saturation was not very good.

1. The presence of a gas effect, likely indicated by a crossover between logs.

2. High values of hydrocarbon saturation within the zone.

It is important to note that within the study area, the presence of radioactive sands can contribute to elevated gamma-ray values. This phenomenon was observed in this specific zone of interest in Sawan 01 well. As a result, the zone was marked as a zone of interest based on the observed gas effect and high hydrocarbon saturation values.

4.6 Petrophysical interpretation of C interval

Petrophysical interpretation of the C Interval of Lower Goru Formation in Sawan 01 and Sawan 07 wells involved loading LAS files for both wells using the Prizm module of Geographix software. In the reservoir zones of interest within the C interval of Sawan 01 well, two zones were identified and marked for further analysis. The interpretation likely included assessing various well logs and petrophysical properties within these zones to understand the reservoir characteristics and potential hydrocarbon saturation.

4.6.1 Petrophysical Interpretation of C Interval Sawan 01

Figure 4.4: *Petrophysical analysis of Sawan-1 C-Interval of Lower Goru Formation.*

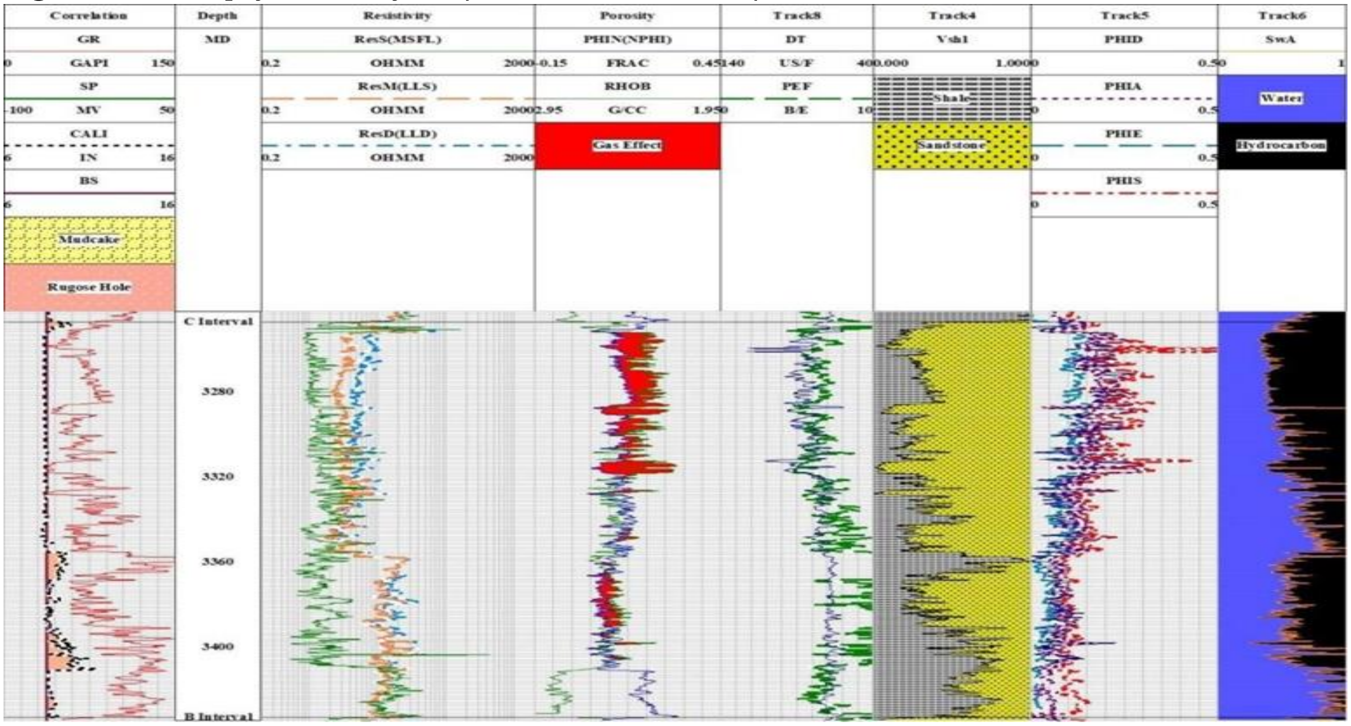

Two zones of interest were marked in the Lower Goru C- Interval of Sawan 01 well. The first zone was observed at the depths of 3268-3387 m, and the second zone was observed at the depth of 3368 to 3387 m.

Within both these zones the gamma ray value was on the lower side, separation between MSFL and LLD was observed. There was presence of gas effect i.e., neutron and density crossover were observed. And lastly the hydrocarbon saturation was also good.

4.6.2 Petrophysical Interpretation of C Interval Sawan 07

Figure 4.5: *Petrophysical analysis of Sawan-7 C-Interval of Lower Goru Formation.*

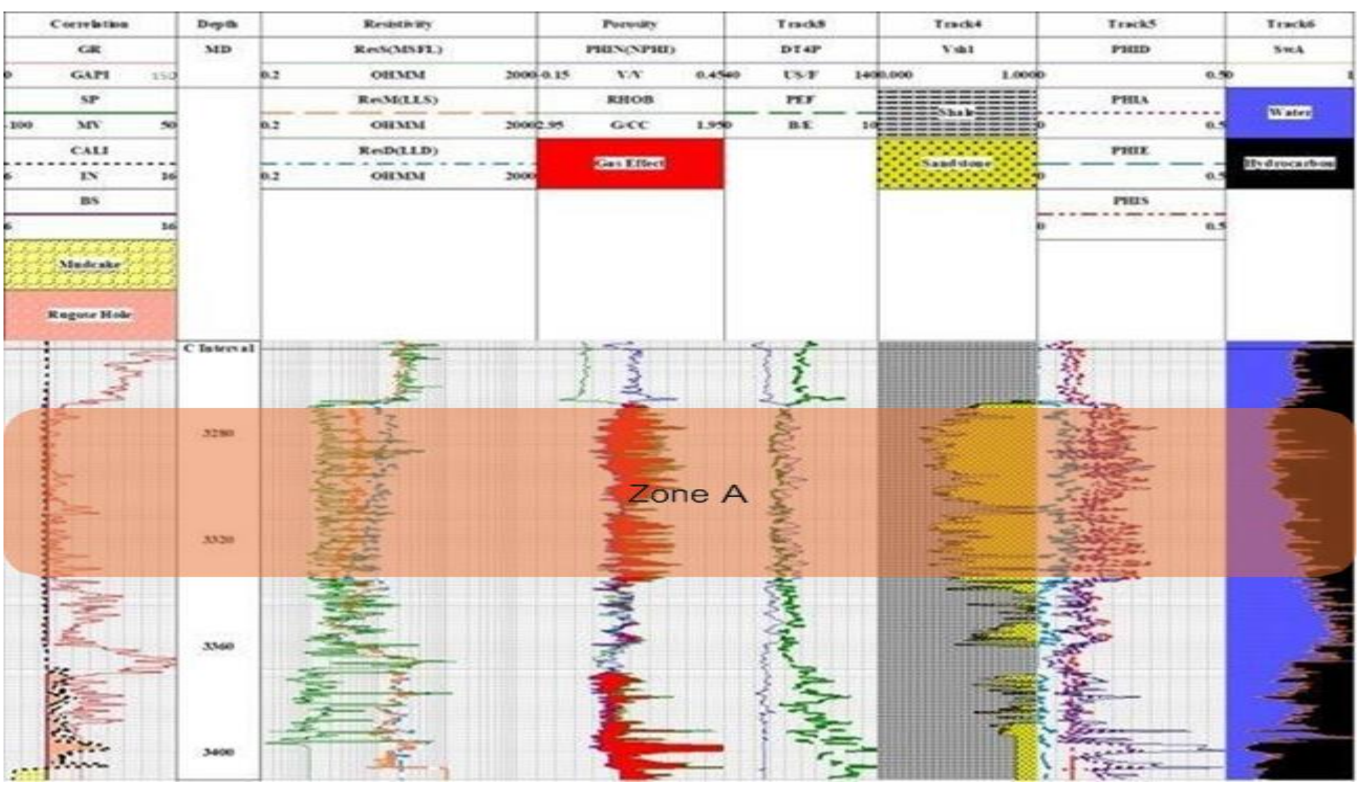

A zone of interest was marked in the Lower Goru C-Interval of Sawan 07 well it was observed at the depth of 3272 to 3335 m.The criteria to mark the zone of interest based on the separation between MSFL and LLD was ruled out. However, within the zone there was presence of gas effect i.e., neutron and density crossover was observed. And lastly the hydrocarbon saturation was also good.

4.7 Results of Petrophysical Interpretation

Table 4.2: *Result of petrophysical analysis of reservoir zones*

Well Name	Hydrocarbon Zone	Depth(m)	Vshl %	PHI %	PHIE %	SwA %	Sh %
Sawan 1 B Interval	Zone A	3486-3487	30	28	28	19	81
Sawan 1 C Interval	Zone 1	3268-3387	10	11	11	19	81
	Zone 2	3368 to 3387	11	10	9.1	61	39
Sawan 7 C Interval	Zone 1	3272 to 3335	1.9	21	17	22	78

Rock Physics and Fluid Replacement Modeling

5.1 Introduction

Rock Physics Modeling is the anticipation of variations in P and S waves and the occurrence of Poisson's ratio. It illustrates the absent log prediction, particularly for S-wave, necessitating the establishment or acquisition of elastic properties. This method aids in forecasting anomalous (mostly density logs) or missing S-wave logs while mitigating uncertainties associated with seismic attribute interpretation. Rock Physics Modeling serves as a crucial parameter in establishing connections between elastic properties like impedance and reservoir velocities (Miguel Bosch et al., 2010).

The correlation between rock properties is elucidated in terms of Elastic moduli, which are subsequently utilized for velocity computations (Wawrzyniak-Guz, 2019).

5.2 Fluid replacement Modeling

Reservoir rock assessment in AVO primarily employs fluid replacement modeling (Ross, 2000; Russell et al., 2003). Fluid replacement facilitates a deeper comprehension of seismic properties and pore fluids, relying on various saturations such as water, gas, and oil (Gassmann’s relation, 1951).

5.3 Workflow of Rock Physics

Figure 5.1: *Fluid Replacement Workflow*

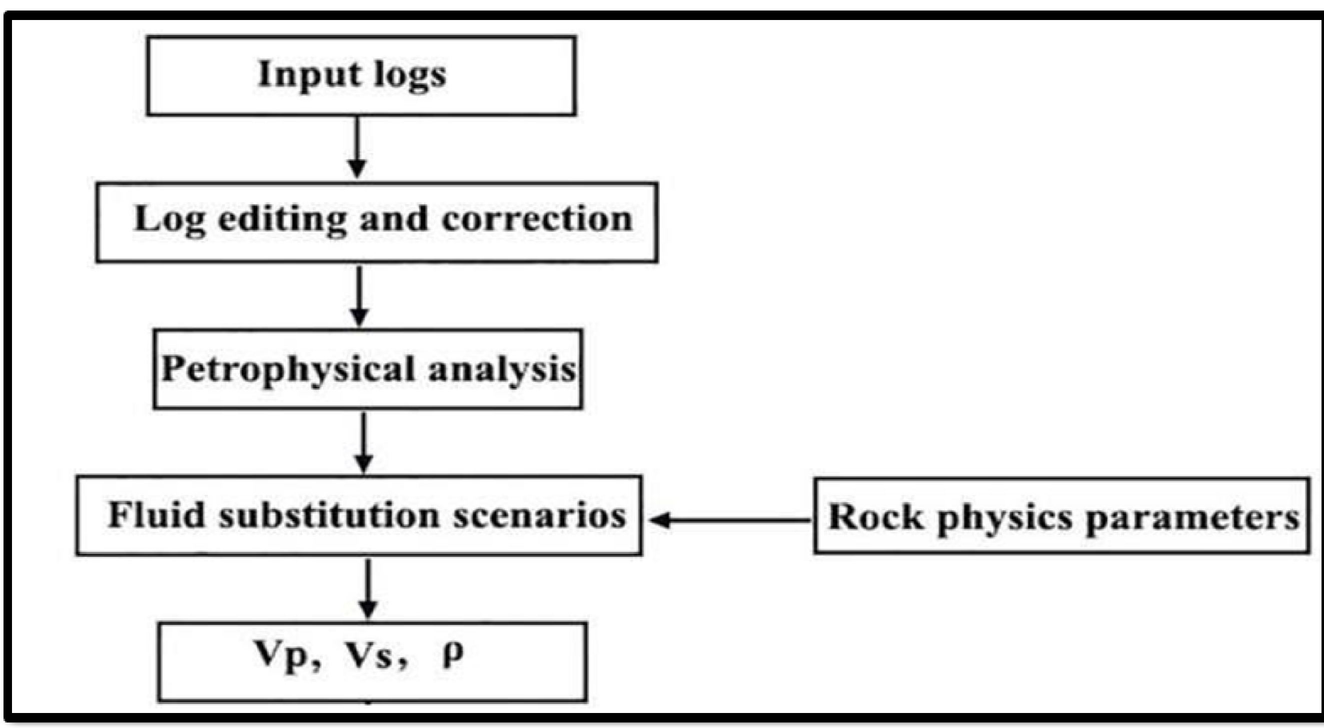

5.4 Scenarios in for Fluid Substitution

Different types of fluids, including water and gas, were introduced and substituted into reservoirs in varying proportions. This approach aimed to evaluate and better assess the quantitative parameters of the appropriate fluids present in the reservoir by depicting amplitude matching. Three primary scenarios were considered:

- Insitu case (80% gas 20% water)
- Gas 100 % and water 0 %
- Gas 50%, water 50%

5.4.1 Insitu Case (80% gas 20% water)

Insitu case we exert 80 % gas and 20% water as substitution method to see the results of the curves how it responds and their variations of behavior.

Figure 5.2: *Depicts that Insitu condition holds substitution of 80% Gas and 20% water scenario.*

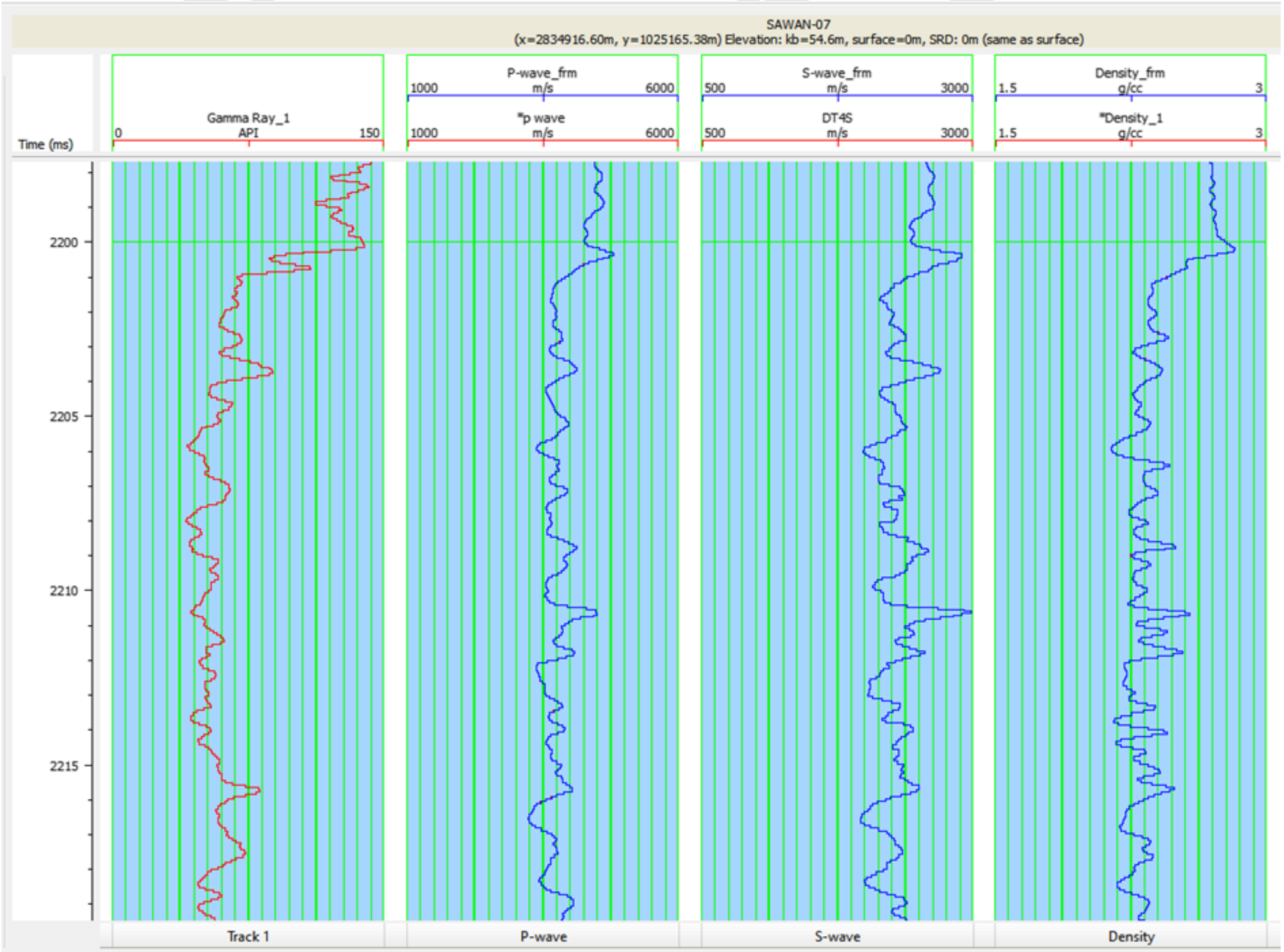

5.4.2 Gas 100% and Water 0%

In Second case we exerted 100 % gas and 0% water as substitution method to see the results of the curves how it responds and their variations of behavior.

Figure 5.3: *Depicts that substitution of 100% Gas and 0% water scenario.*

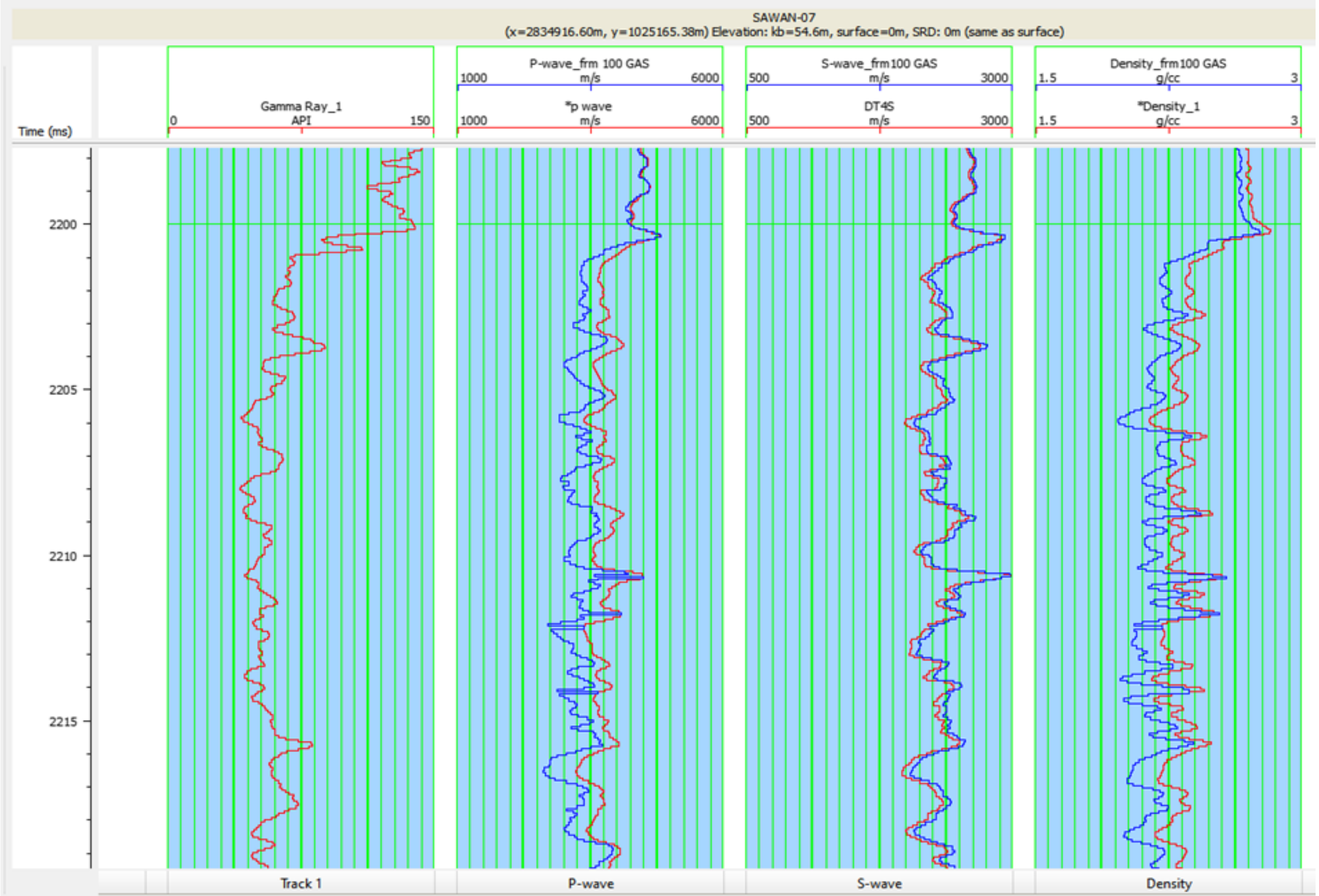

5.4.2 50% Gas 50% Water Case

In Third case we exerted 50 % gas and 50% water as substitution method to see the results of the curves how it responds and their variations of behavior.

Figure 5.4: *Depicts that substitution of 50% Gas and 50% water scenario.*

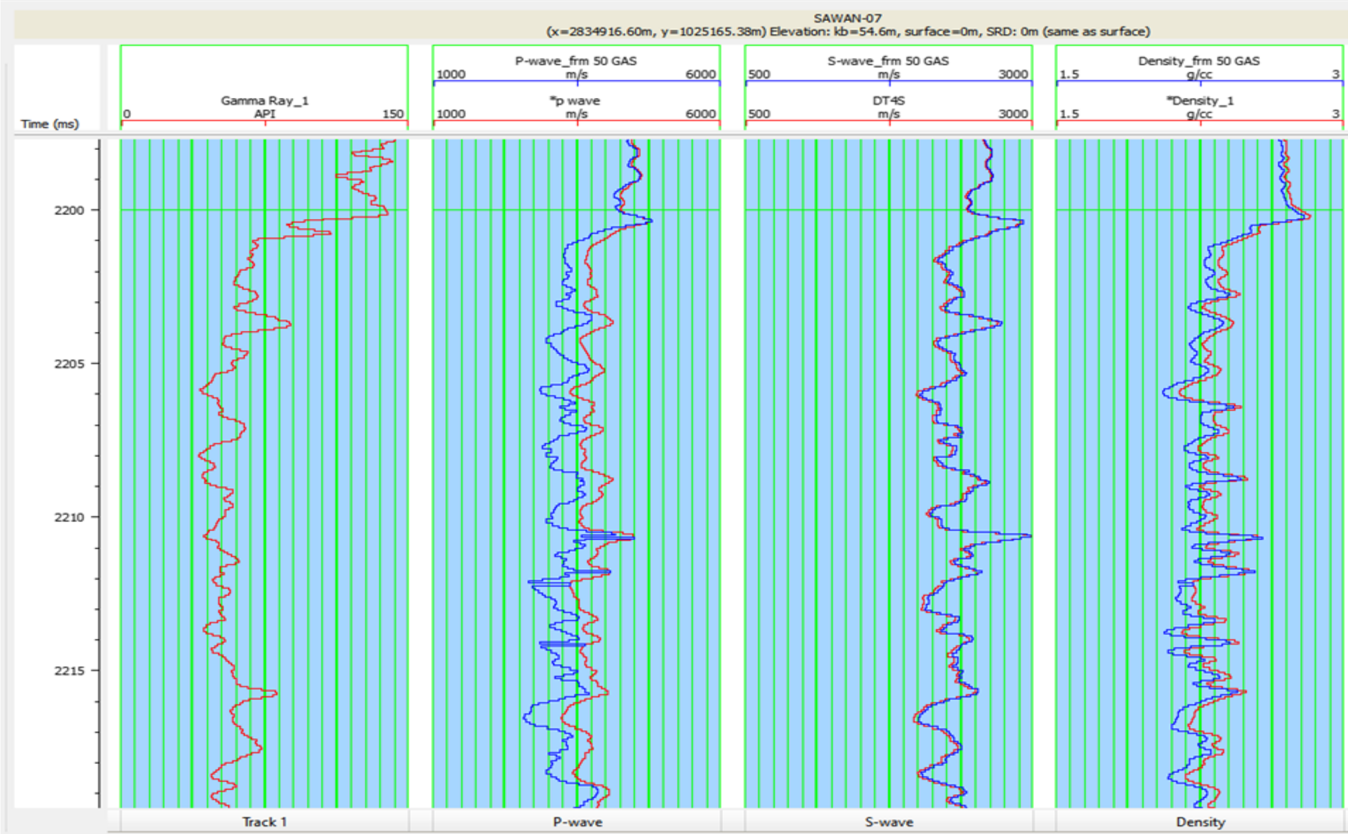

5.4.4 Outcome

As shown in the figure we have substituted different scenarios and exerted values and made S-Wave Prediction. Lower Goru C Sand interval is acting reservoir and have lot of potential to act as reservoir.

Seismic Inversion Technique for Reservoir Characterization

6.1 Introduction

Seismic inversion, which is a subsurface geological modelling approach uses well-data as a control and seismic data as an input. The seismic inversion is carried out by converting the data in amplitude form to the impedance form (Kianoush et al., 2023). Seismic inversion enhances interpretation by helping to identify the significant subsurface geological and petrophysical boundaries (Talib et al., 2022). Seismic inversion is one of the known methods for extracting valuable information from seismic data, interest in it has been growing steadily over the past few years. Seismic inversion also enhances the resolution of conventional seismic. Deterministic and probabilistic are the methods of inversion and the approaches are either pre or past stack (Veeken and Silva, 2004).

Earth's properties are reconstructed by seismic inversion, and it is readily employed in the industries of oil and gas. For the prediction of porosity and lithology it combines well data and seismic data. These characteristics of rock may be applied for the identification of hydrocarbons and reservoirs (Kianoush et al., 2023).

Figure 6.1: *Generalized workflow of seismic inversion (Veeken and Silva, 2004).*

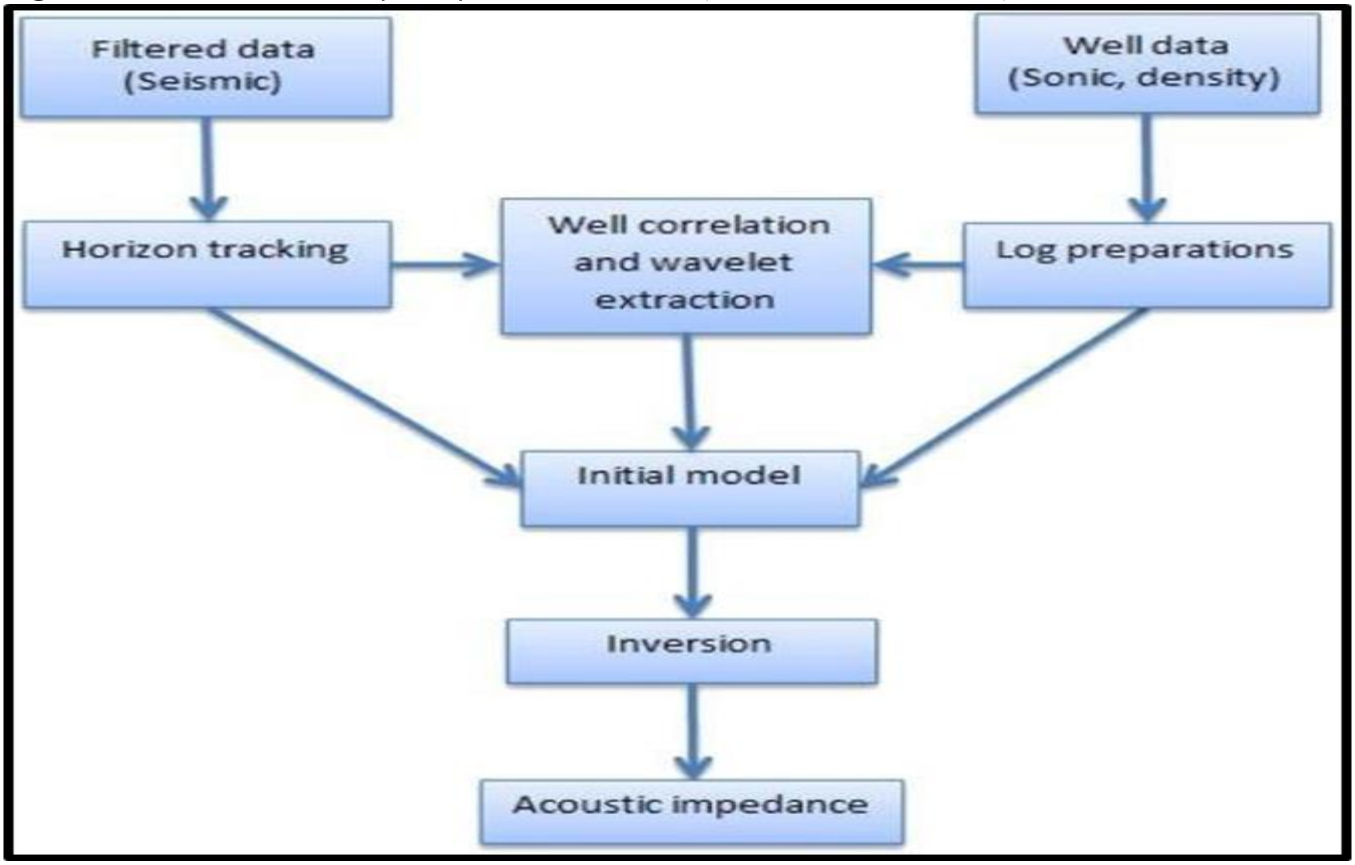

Pre-stack seismic data and post-stack seismic data are the two types of seismic data that the seismic inversion method deals with. Both pre-stack seismic and post-stack seismic data are used in seismic inversion methods (Kumar et al., 2016). Post-stack seismic data only produces P impedance, whereas pre-stack seismic data also generates P and S acoustic impedance as well as their derivatives, such as Vp/Vs, Lambda-rho, and Mu-rho, which can be used to estimate fluid and lithology parameters from the subsurface (Barclay, 2008). However, post stack inversion is performed in this research.

6.1.1 Seismic inversion's purpose

The main objective of seismic inversion is to convert seismic reflection data into quantitative rocks properties that describe the reservoir. Acoustic impedance logs are calculated at each CMP in their most basic form (Barclay, 2008). Results using inversion improve resolution and support more precise interpretation as compared to working with seismic amplitude. This then makes it easier to estimate the reservoir characteristics like porosity and net pay (Pendrel, 2001).

Other advantages of seismic inversion include:

- Wavelets impacts within the seismic bandwidth are eliminated by using seismic inversion (Kianoush et al., 2023).
- Overburden is separated from reservoir properties.
- Impedance domains interpretation is typically simpler than seismic domain interpretation (Kianoush et al., 2023).

6.2 Model Based Inversion

In the geophysical community, model-based seismic inversion is very common because it provides quick and accurate estimations of acoustic impedance. In a model-based inversion, the wavelet is convolved with the simplistic initial acoustic impedance model to produce a synthetic response that is compared to the actual seismic trace (Kianoush et al., 2023).

To create a synthetic seismic trace, using this method, the seismic trace (initial model) is convolved with a wavelet. Next, until the difference between the initial trace and invented trace is decreased to a limit value, the image is subjected to numerous iterations (Russell, 1988).

$$J = weight\ a\ x\ (S - W * R) + weight\ b\ x\ (M - H * R)$$

The seismic trace is denoted by S in the equation, the wavelet recovered from seismic data is donated by W, the reflectivity series is denoted R, the initial model is donated by M and H is integration operator (Russell, 1988).

Given the initial half of the equation is obviously modelled with seismic trace while the other part is modelled using an estimated initial model. Seismic trace was modeled in the first quarter of equation and the estimated impedance was modelled in the second portion (Russell, 1988).

6.3 Methodology adopted for Model Based Inversion

The model-based algorithm of post stack inversion is performed by using Hampson and Russell software. The methodology utilized for conducting the model-based seismic inversion is outlined in the workflow provided below (Figure 6.2).

Figure 6.2: *Workflow Adopted for Modal Based Inversion*

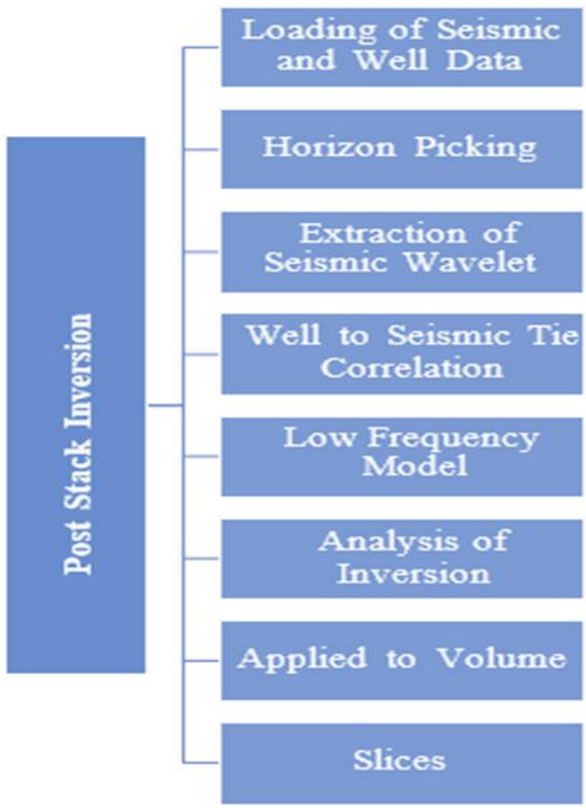

6.3.1 Seismic and Well Data Loading

The loading of seismic and well data into Hampson and Russell software is the first step in post-stack inversion. The 3D cube of Sawn Gas Field is loaded into the software along with interpreted well data in Las format, following data loading the location of well is matched with seismic data for confirming the exact location of well in the seismic cube.

6.3.2 Loading of Horizons

The next step involves loading of horizons in the seismic section. The interpreted horizons are exported in time amplitude format from Kingdom Software. After that these horizons are imported in HRS software. The horizons of B and C intervals of Lower Goru Formation were imported.

6.3.3 Extraction of Statistical Wavelet

One of the most important steps in quantitative interpretation is wavelet estimation. The outcomes of seismic inversion depend on the quality of the wavelet, which in turn determines the quality of the seismic correlation. The seismic wavelet is an essential link between seismic data and subsurface stratigraphy and rock characteristics (Cui et al., 2014).

6.3.4 Seismic to Well Correlation

This study employs the sonic (compressional wave velocity) and density logging information from the Sawan-07 well to estimate the acoustic impedance of the subsurface strata. This is then aligned with the seismic data from In-line 791 for a comparative analysis as illustrated in Figure 6.6.

Figure 6.3: *Correlation of seismic data with Sawan-07 well.*

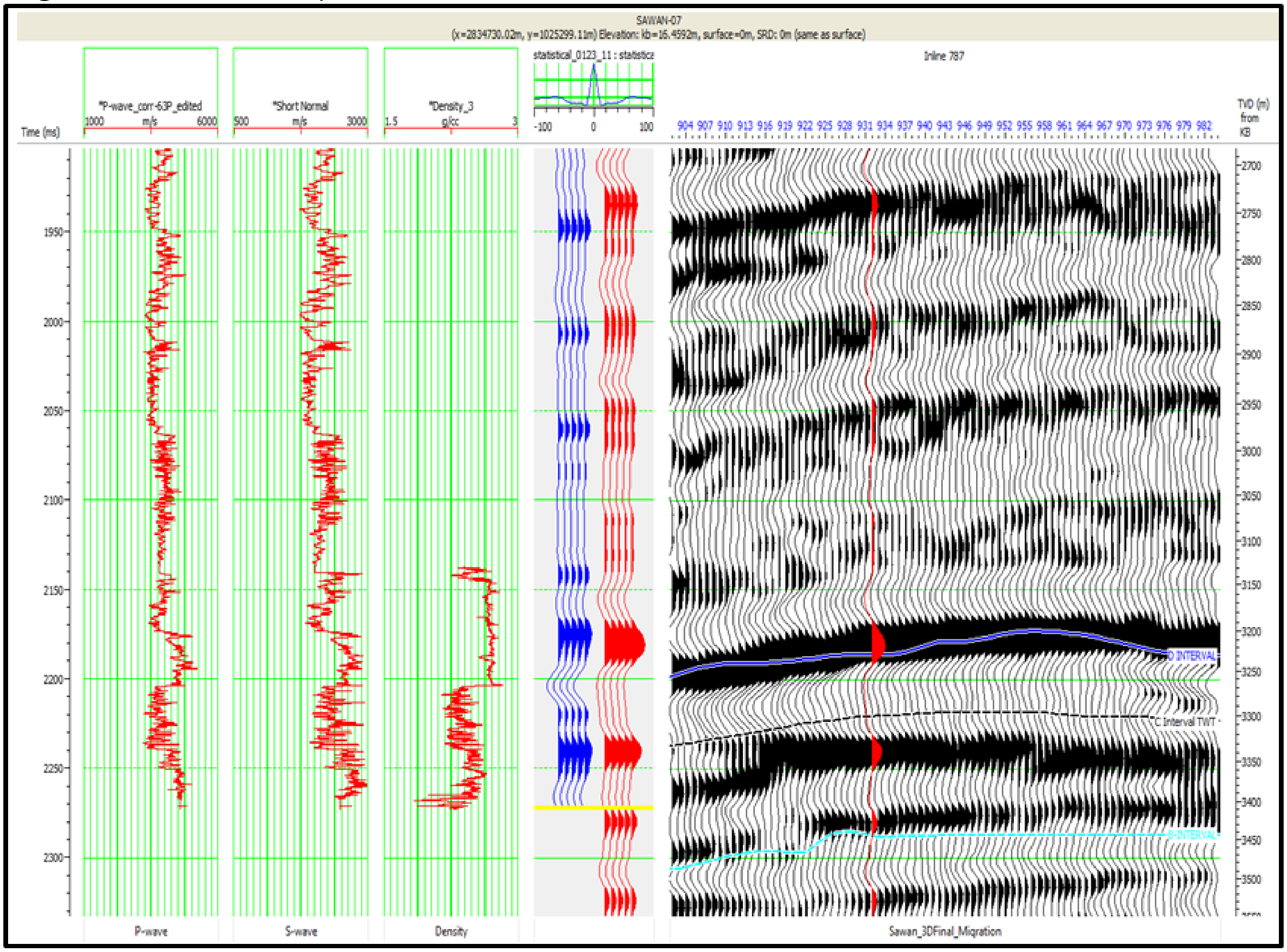

6.3.5 Initial Low Frequency Model

The initial low frequency model is estimated using acoustic impedance. The acoustic impedance is divided into 2 types namely relative and absolute acoustic impedance (Sams and Carter, 2017). It is not necessary to create a low frequency model to calculate the relative acoustic impedance. Because of the relative qualities of the strata, it is favorable for qualitative interpretation of seismic sections (Li et at., 2013). Integration of low frequency model during seismic inversion improves the qualitative and quantitative interpretations levels of seismic inversion results. Well data Information is required to build low frequency model. The qualitative and quantitative interpretation gets enhanced by integrating low frequency model during the seismic inversion (Kumar et al., 2016).

Figure 6.4: *Low Frequency model with well location of Sawan-07*

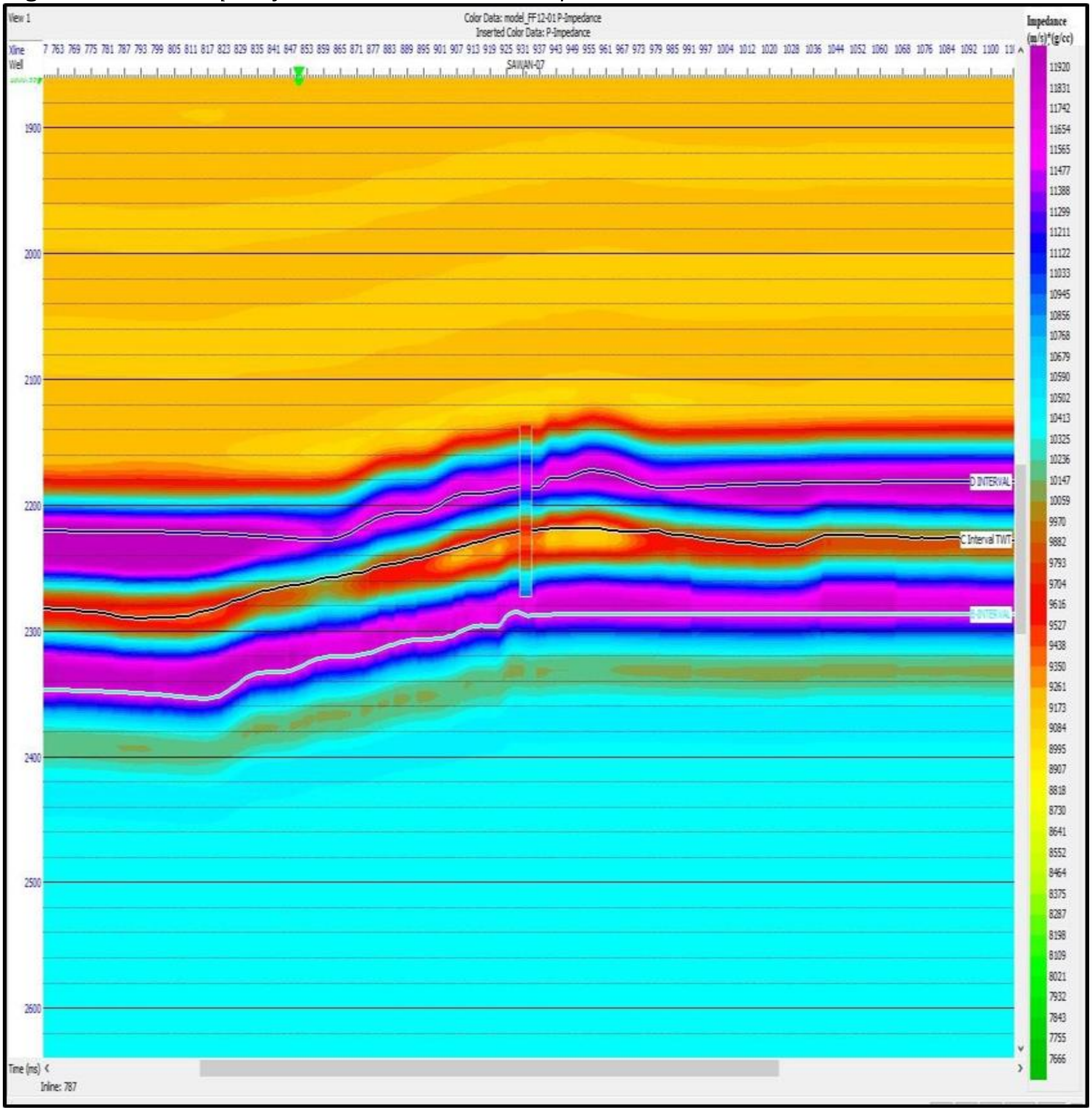

The low frequency model of lower Goru formation shows in figure 6.4. In this model all three intervals B and C are marked and displayed with different acoustic impedance contrast. B interval which is purple according to scale bar having higher impedance value ranging from 11388 to 11920 g/cm3-m/s, and C-Interval is showing low impedance values ranging from 8641 to 10059 g/cm3-m/s,

6.3.6 Inversion Analysis

At the Sawan-07 well site, the given seismic cube information was analyzed for model base inversion. The wavelet that was extracted from the time window was between 2200 to 2600 ms. The wavelet that was extracted seismically was adjusted by comparing the synthetic trace with the inverted trace at the well location. A good impedance model will be generated as a result of high correlation percentage. As seen in Figure 6.5 the black color represents the traces and synthetic traces are shown by red color. Sawan-07 is having correlation coefficient of 99.76% with root mean square error between the seismic trace and synthetic is 0.2%.

Figure 6.5: *Model based inversion analysis of Sawan-07*

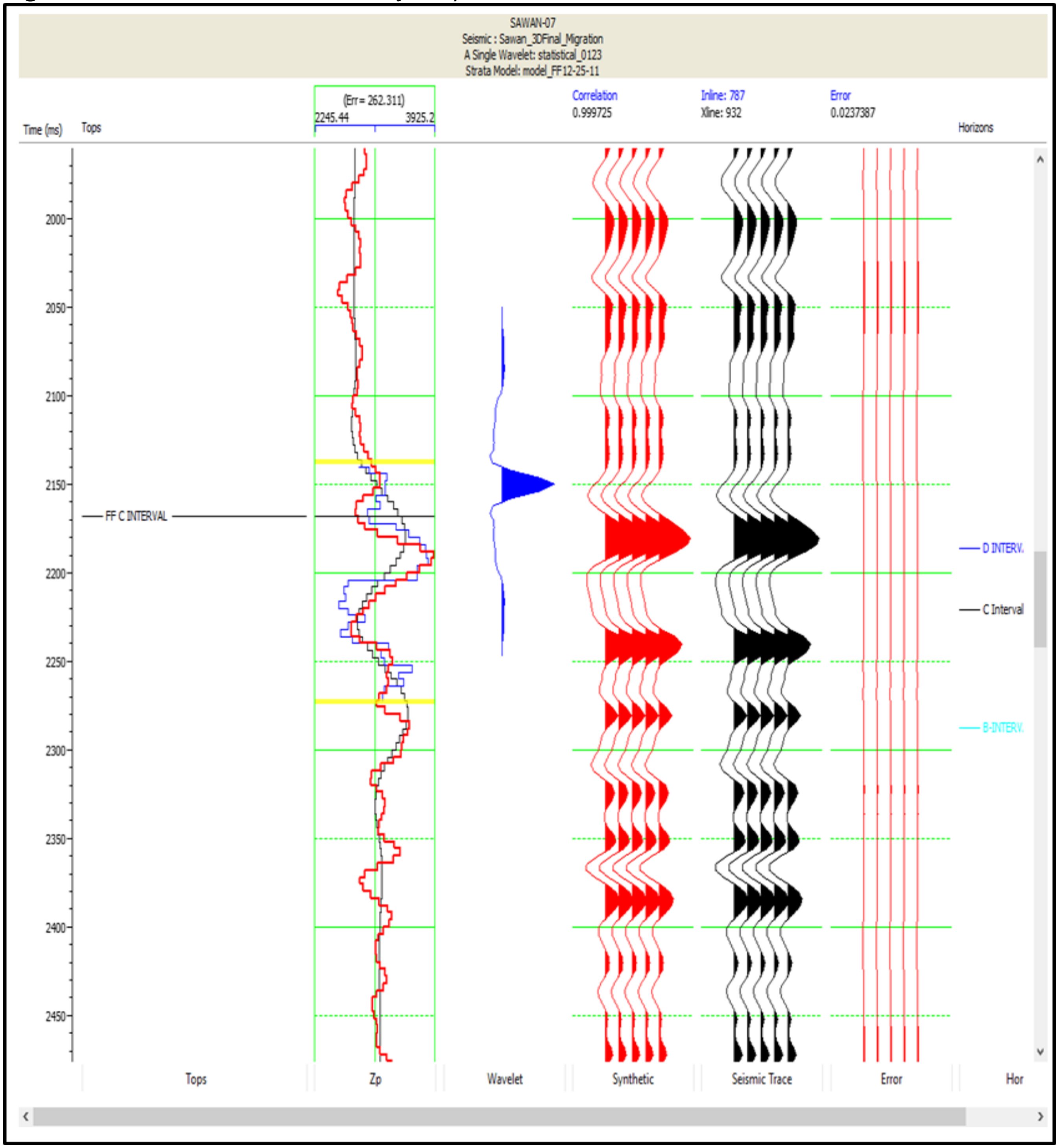

6.3.7 Results of Model Based Inversion

Physical properties of rock and fluids from seismic data are extracted by seismic inversion (Krebs et al., 2009). The mapping, interpretation, and quantification of hydrocarbon bearing zones have become less challenging by using seismic post stack inversion (Ali et al., 2018). The post stack inversion with zero offset converts seismic data(amplitude) into volume of acoustic impedance contrast by using geological data, seismic, well logs etc. (Downton et al., 2005).

Model-based inversion produces an acoustic impedance model that matches the entire frequency range of impedance by taking low frequency model and seismic data as inputs. The model-based inversion is more realistic and accurate, but an accurate initial model and computation is required for model-based inversion (Narayan et al., 2023).

Figure 6.6: *Final Computed impedance model at Sawan-07 Well location.*

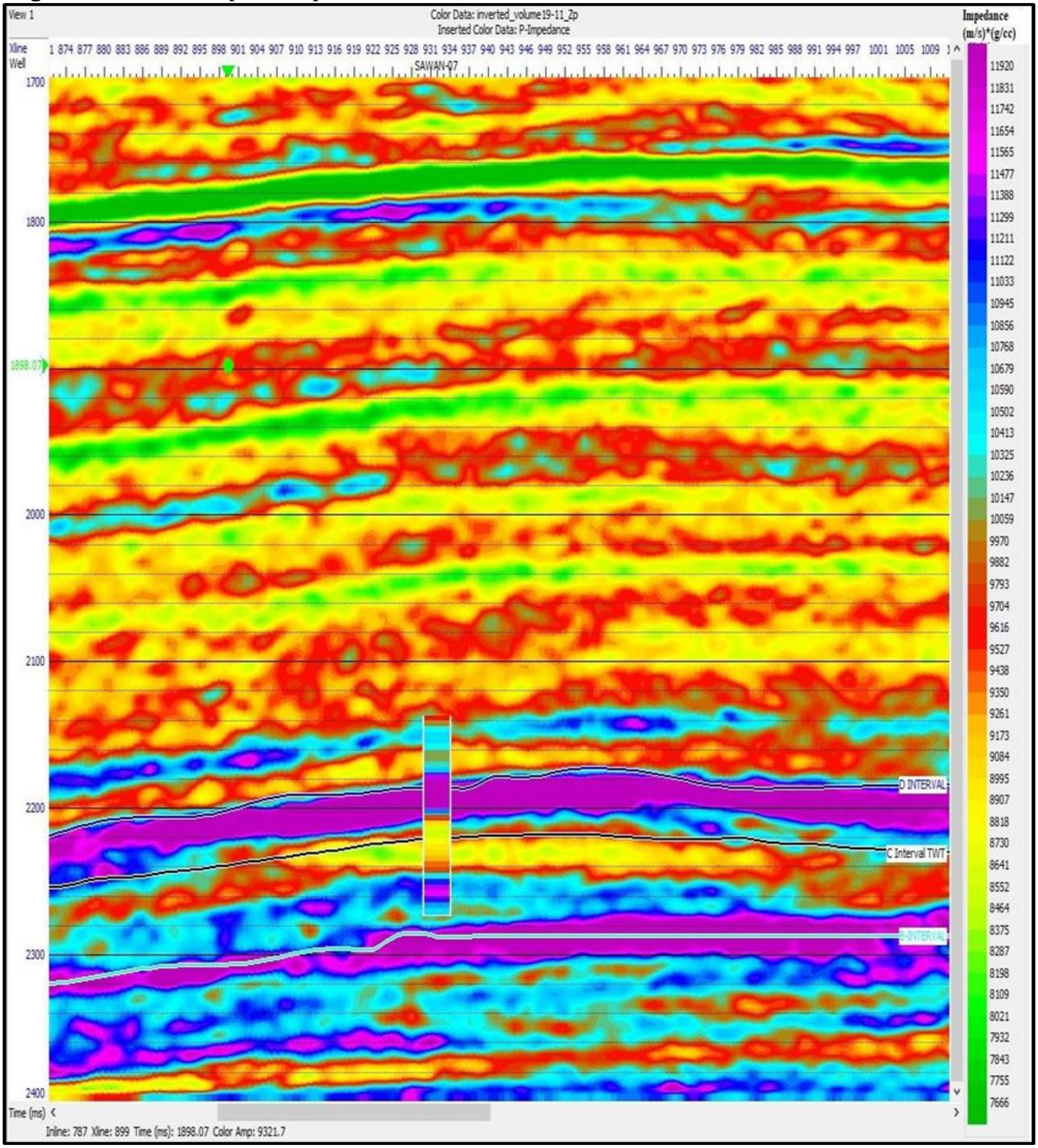

As can be seen in Figure 6.6 the impedance range lies between 7666 to 11920 g/cm3-m/s. And the C interval of Lower Goru Formation is marked by the impedance of approximately and 12687 g/cm3-m/s respectively. Considerably lower impedance values are encountered along the horizons. The low impedance indicates the reservoir zones and might be having gas saturation.

The inverted impedances of well and seismic sections are exact match shows in figure 6.9. the well impedance is placed on time section for confirmation.

6.3.8 Slice of C interval

A 3D slice was generated for the C interval within the Lower Goru Formation (Figure 6.7). This slice displays the overall variation in P impedance across the C interval. Impedance values within the C interval range from 5273.28 to 13102.55 g/cm3-m/s.

Figure 6.7: *3D cube slice for C Interval showing variation for P-Impedance.*

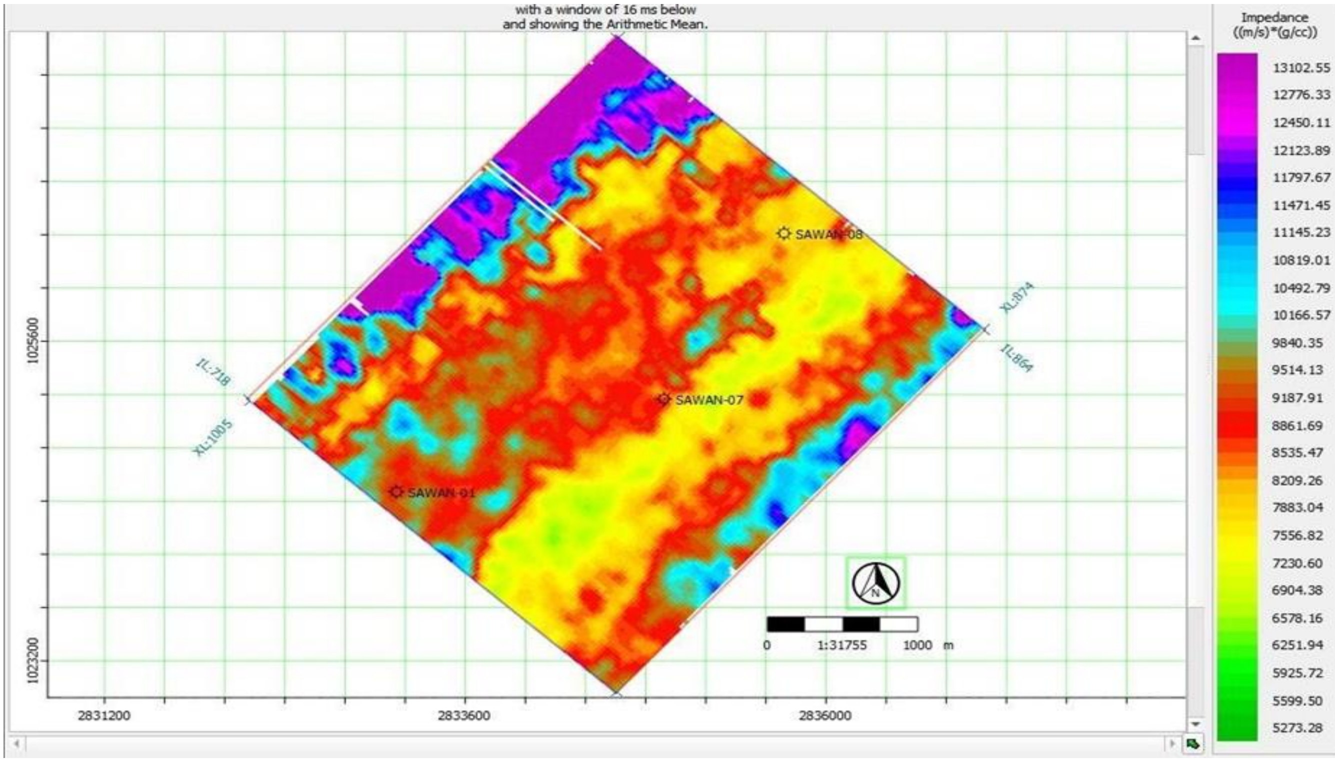

Notably, along the Sand channel (C sand), there is a significant anomaly of lower impedance observed at the Sawan-01 and Sawan-07 locations, suggesting a possible accumulation of hydrocarbons (gas). This observation is depicted in Figure 6.7, where relatively higher impedance values are noted in the northern-western and some eastern areas, while lower values are observed centrally and at the locations of Sawan-01 and Sawan-07. These lower impedance values are indicative of potential hydrocarbon accumulation.

Machine Learning Implementation for Reservoir Characterization

7.1 Introduction

Machine learning has played a momentous role in the hydrocarbon industry in the last couple of years. Machine learning algorithms will have outstanding results to depict the reservoir characterization by doing firstly Exploratory Data Analysis (EDA) and then comes towards machine learning.

The main Problem starts from Data acquisition problems then Seismic processing like noise removal etc. So, during such setups important data is missed in which we do seismic interpretation and petrophysical analysis. So, to enhance the results we will apply a machine learning approach towards it.

7.2 Methodology

By using Probabilistic Neural Network (PNN) we have calculated Volume of Clay, Porosity and Saturation.

7.2.1 Probabilistic Neural Network (PNN)

PNN is widely used for several years in geophysical studies. It depicits the distance of weighted substance approach to the tiny points for the interpolation (Mahmood et al., 2017).

7.2.2 Volume of Clay prediction using PNN (Machine learning)

Clay plays a vital role in hydrocarbon industry as its minerals plays momentous role in the composition in source rocks as well as reservoir rocks which ultimately is produces and store hydrocarbons. Clay minerals affect the physiology and chemistry of sandstone, limestone’s and unconventional shale. We have predicted volume of clay by using PNN.

Figure 7.1: *Cross plot of Actual Volume of Clay and Predicted Volumetric analysis of Clay (modeled).*

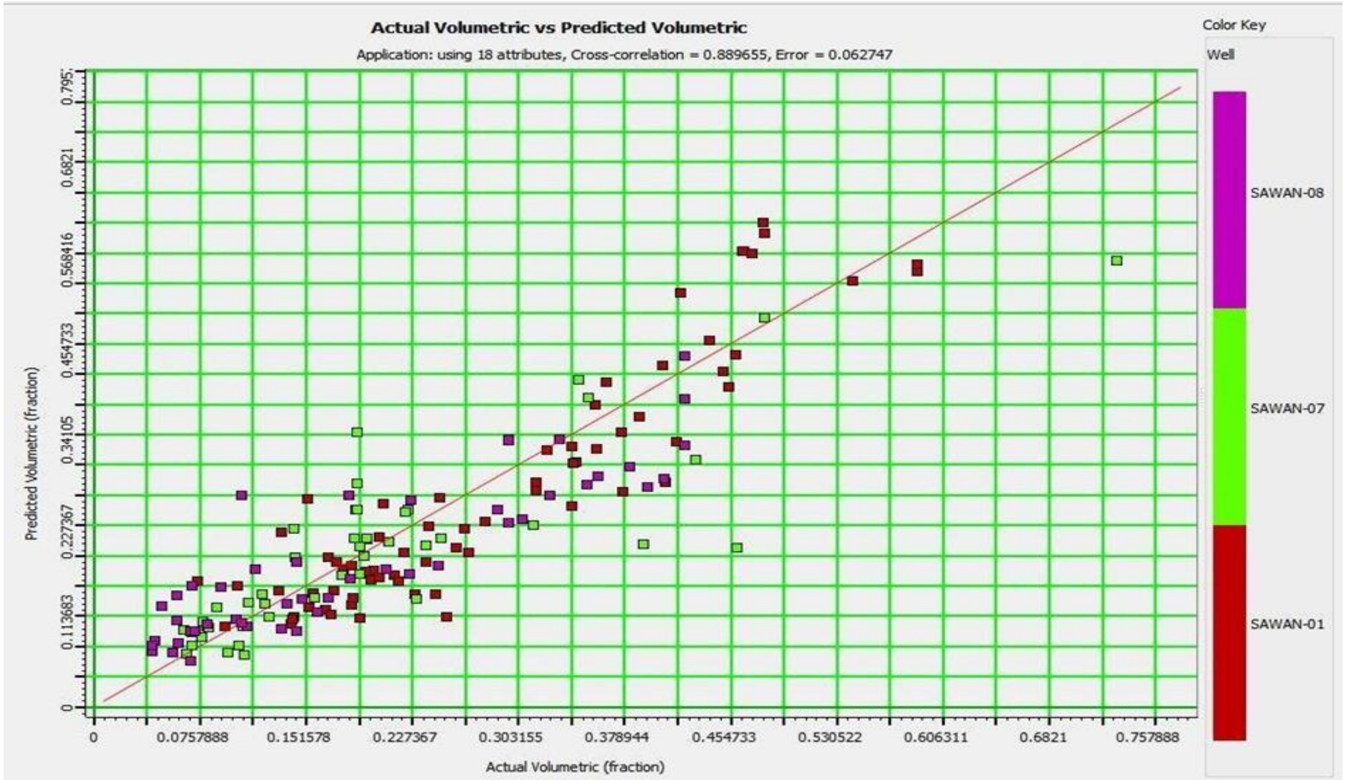

Figure 7.2: *Training result of PNN of Actual Volume of Clay and Predicted Volumetric analysis of Clay (modeled).*

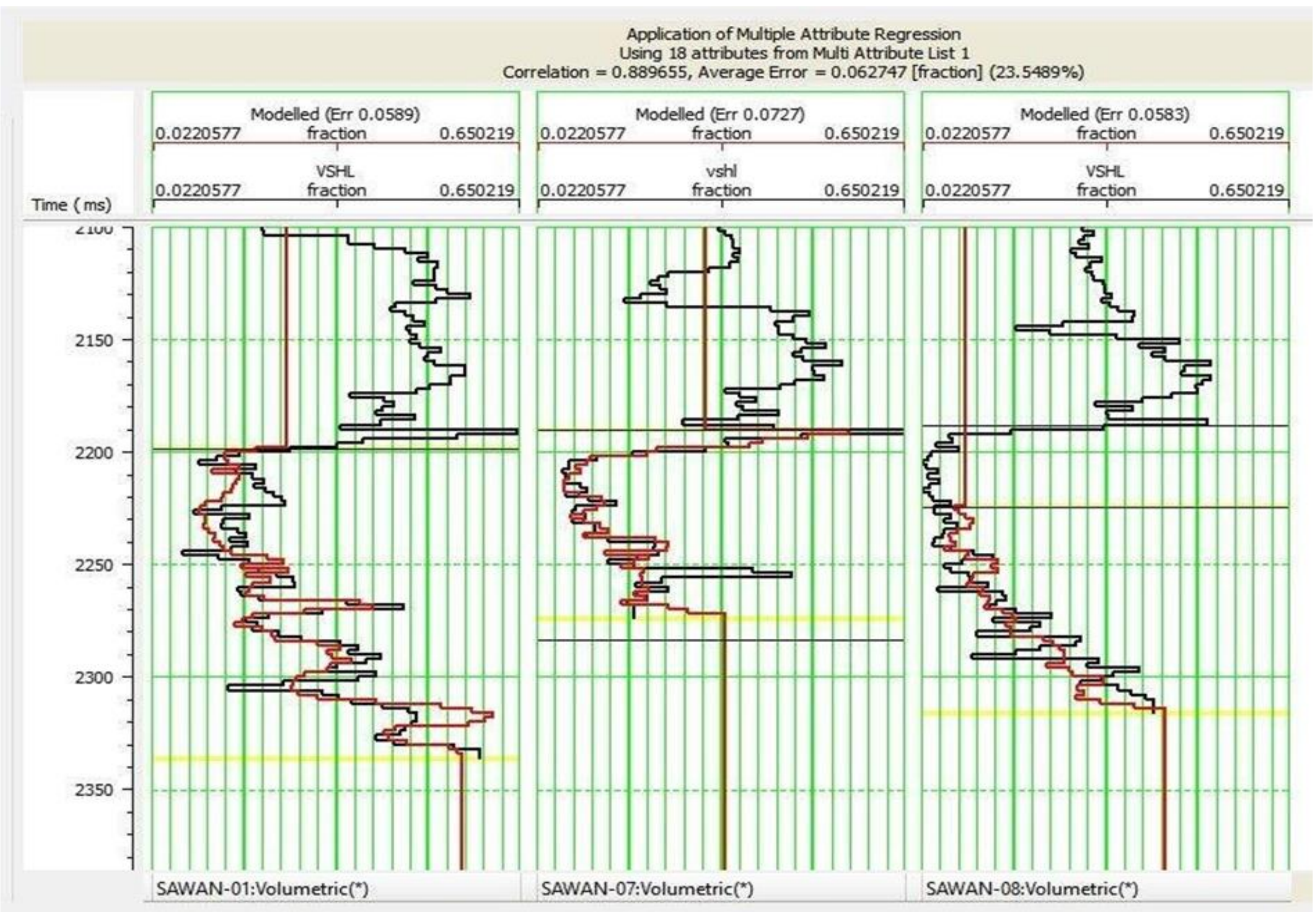

7.3 Results

The correlation between Actual (Black, Petrophysically calculated) and Predicted (Red, PNN) volumetric assessment is 96% - 97% while factor of error is 0.3 to 0.4% which is negligible, so we have enormous sort of results.

Figure 7.3: *Depicts that values ranging from 0.62 % to 0.68% which is holds very good results of C sand in Sawan-07.*

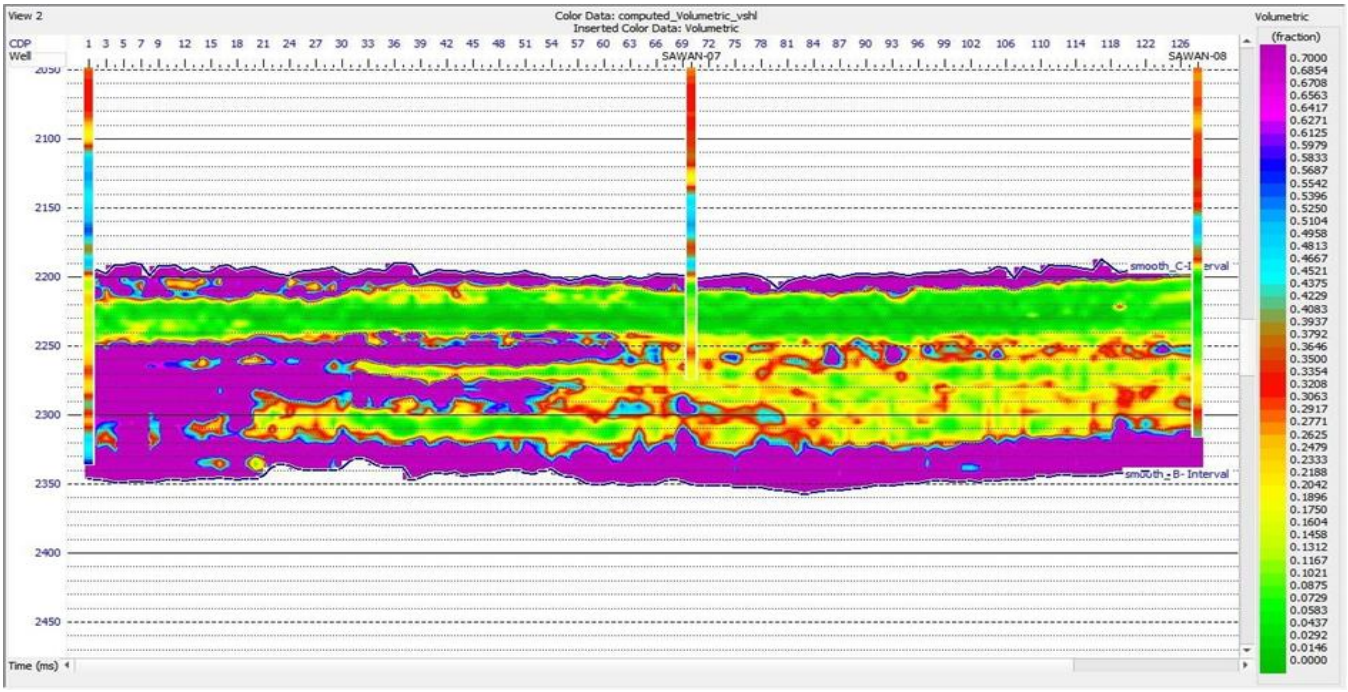

7.3.1 Porosity prediction using PNN (Machine learning)

Estimation of porosity occurs from the inverted impedance and comparison occurred between actual porosity and modeled (predicted).

Porosity is predicted by probabilistic Neural Network. Correlation plot results of PNN for here is as follows in Figure 5.16. Actual porosity is showing good results in Modeled porosity and correlation is about 97%.

Figure 7.4: *Training result of PNN modeled porosity(red) and actual porosity (black).*

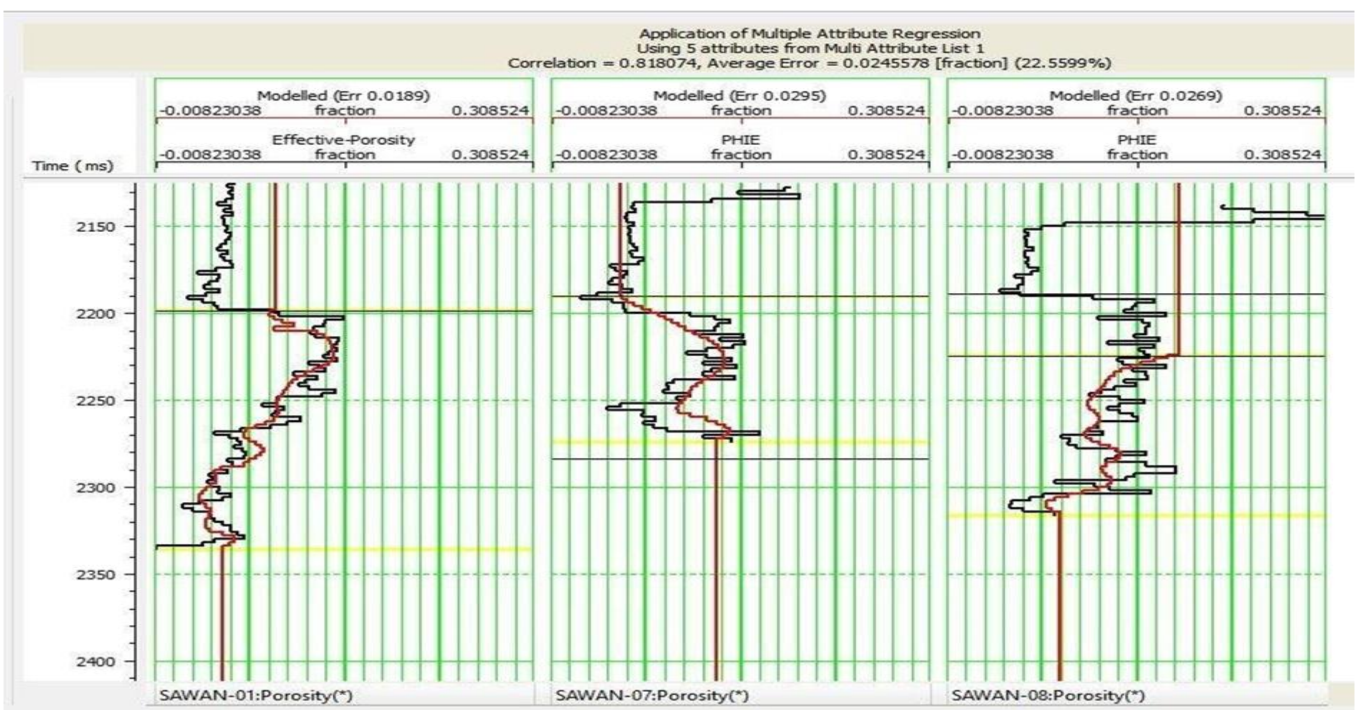

Figure 7.5: *Cross plot of actual porosity and predicted porosity (modeled).*

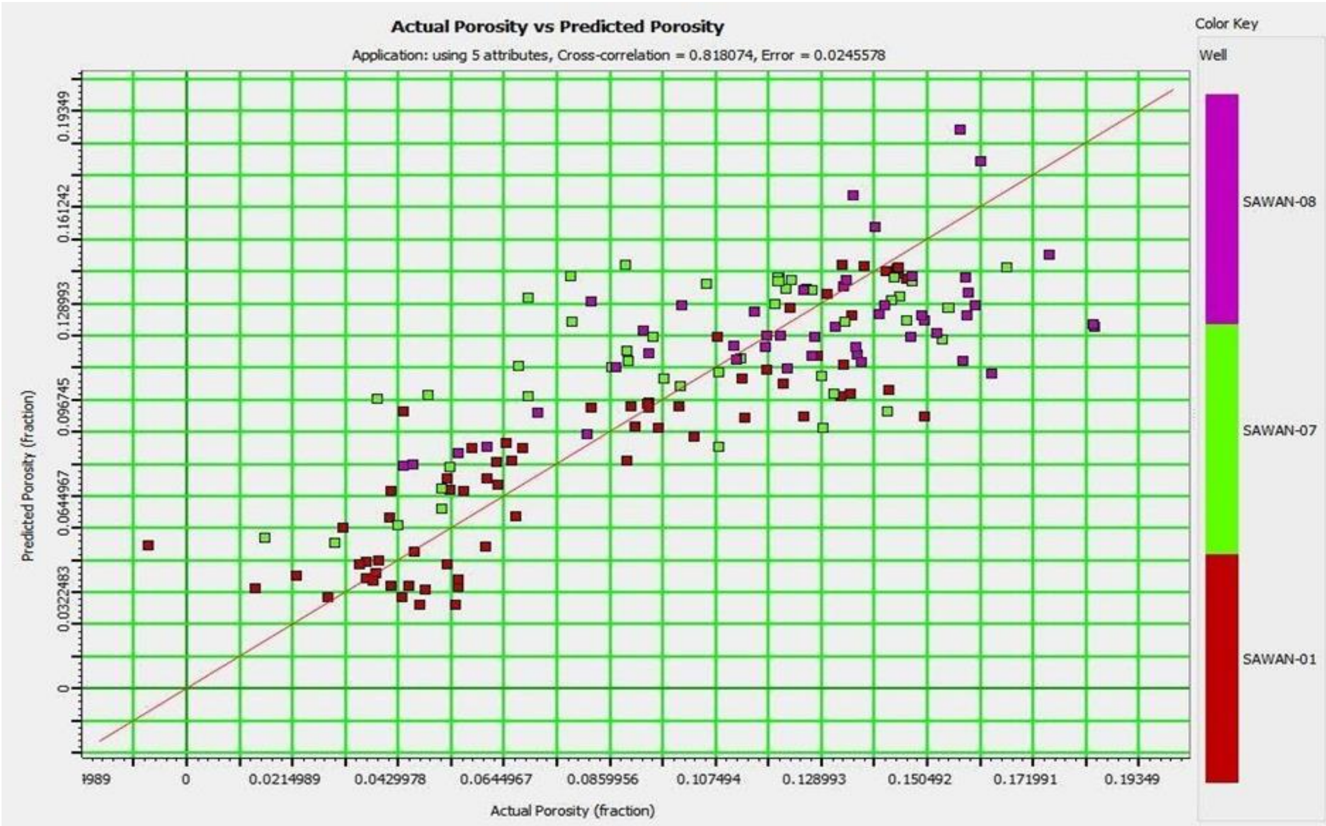

Figure 7.6: *Depicits that values ranging from 0.203 % to 0.215% porosity which is holding very good results of in C interval in Sawan-07.*

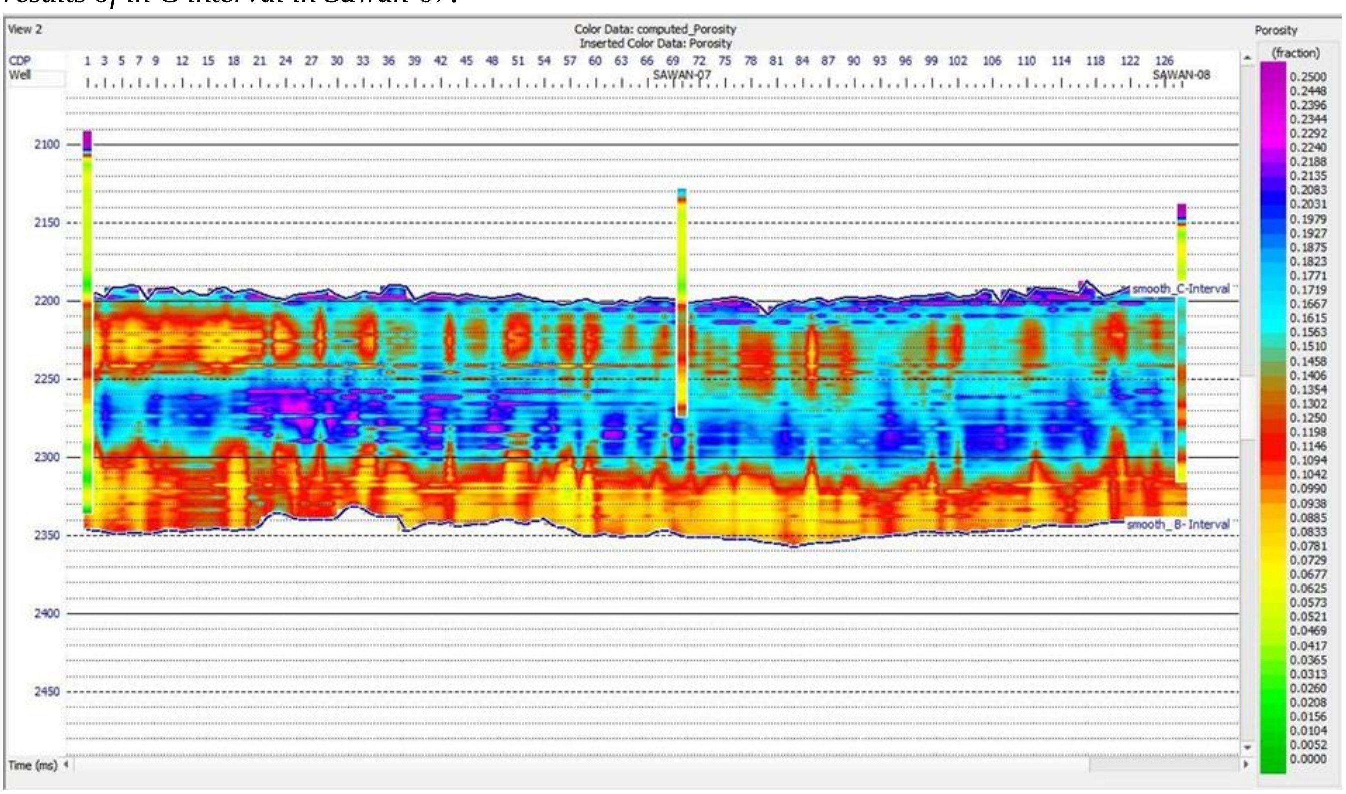

7.3.2 Sw prediction using PNN (Machine learning)

Saturation of water is important parameter to depict Hydrocarbon potential of reservoir. As (1-SH = SW). So training error is 12% only which is negligible.

Figure 7.7: *Training result of PNN modeled Saturation of Water, actual Saturation of Water.*

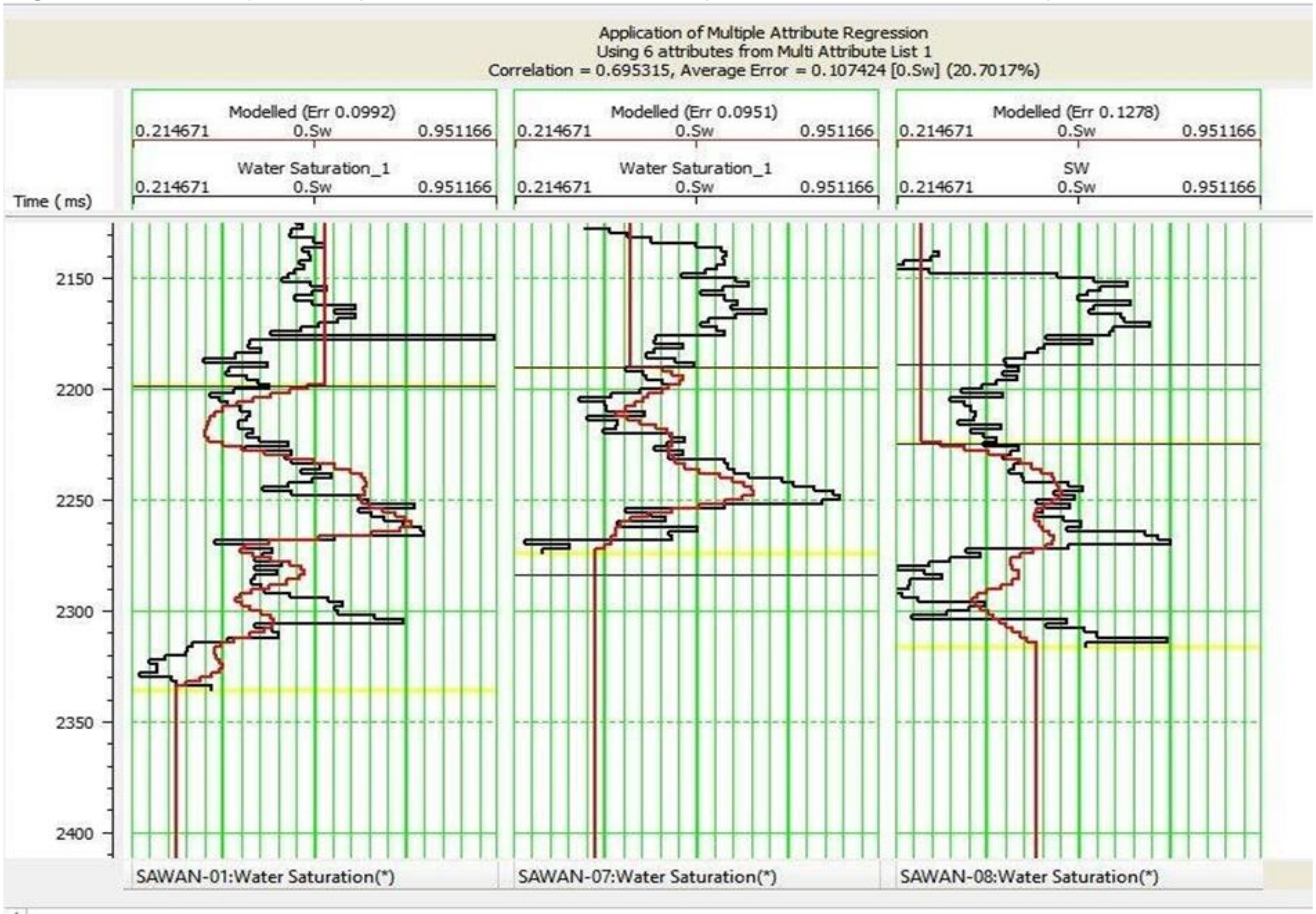

Figure 7.8: *Cross plot of Actual Water Saturation with Predicted Water Saturation (modeled).*

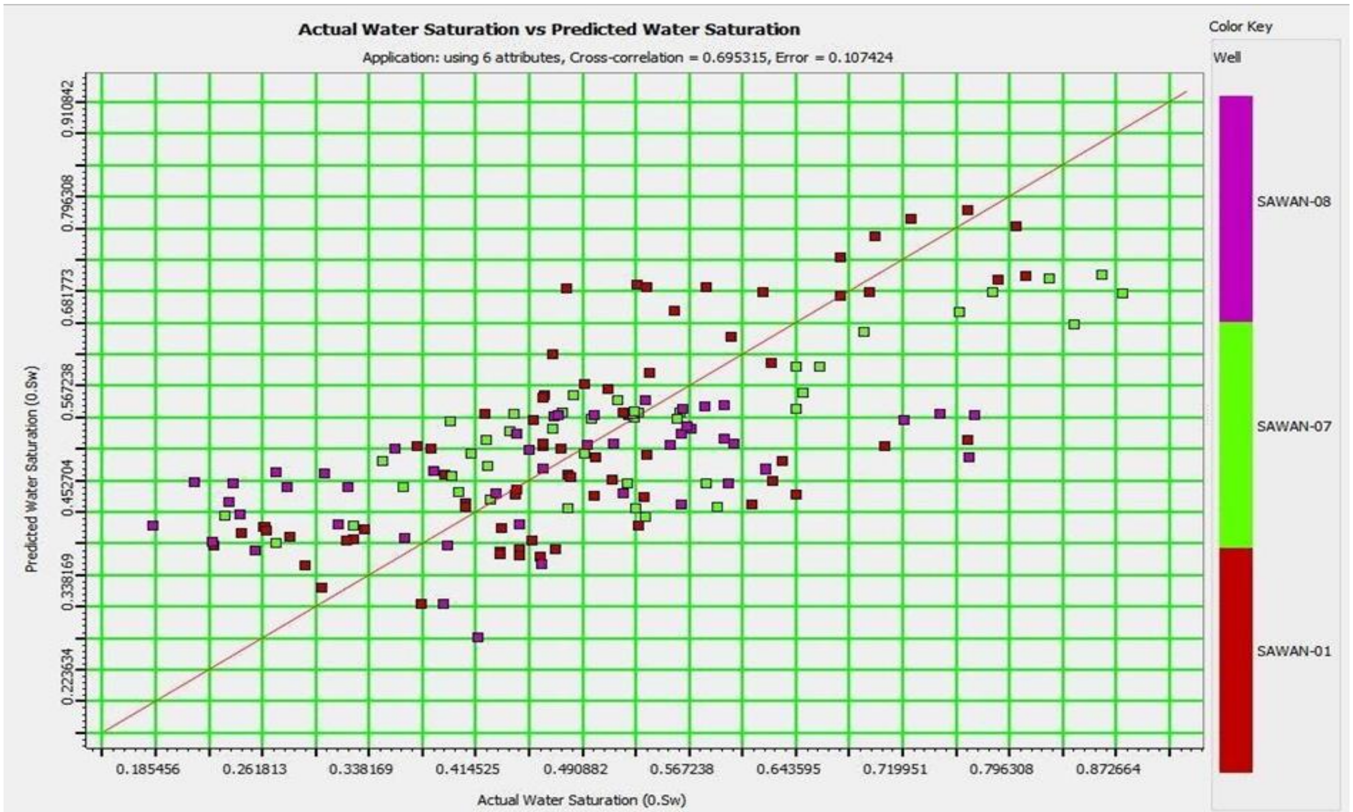

Figure 7.9: *depicits that values ranging from 0.31% to 0.42% of predicted water Saturation which is holding very good results of C sand interval in Sawan-07.*

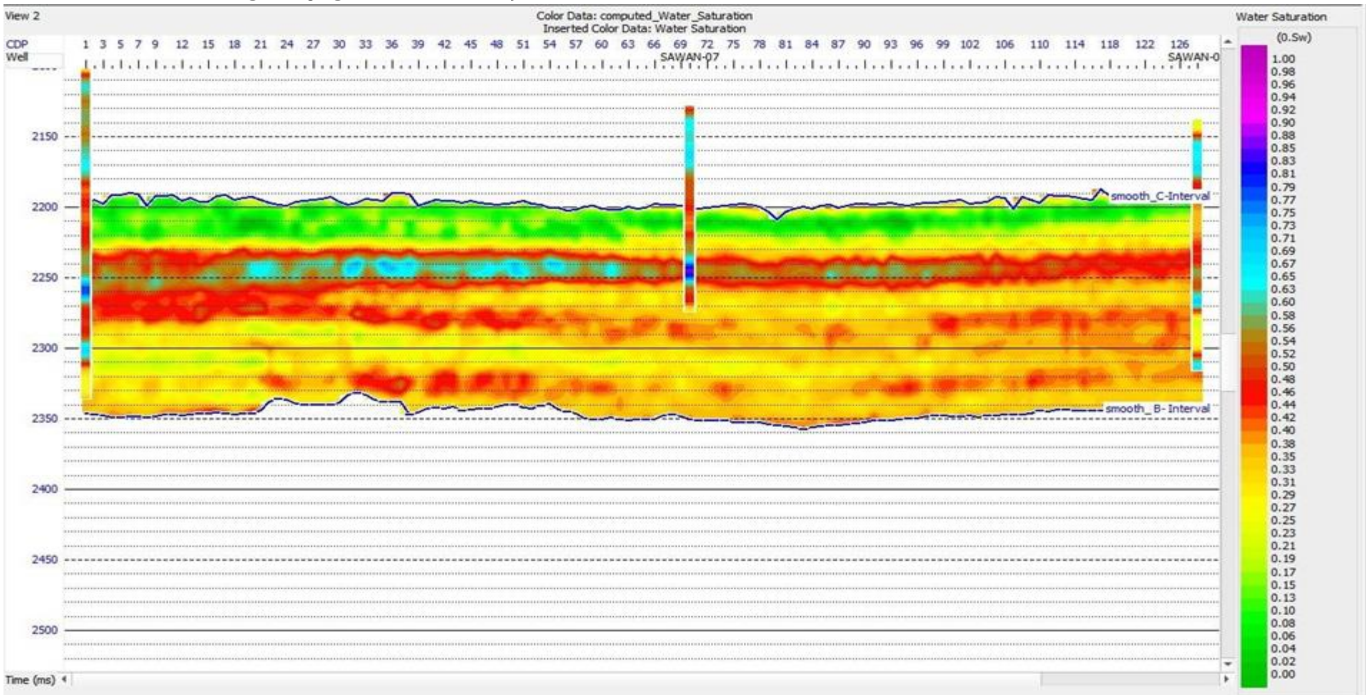

Conclusions

1. 3D seismic interpretation has revealed that the study area is located in an extensional tectonic setting, characterized by the presence of two clearly defined normal faults on the seismic section. Additionally, when examining the time and depth contour maps, it becomes evident that the C interval exhibits a more pronounced behavior in terms of hydrocarbon presence compared to the B interval.
2. The petrophysical analysis of both Sawan 01 and Sawan 07 wells has identified distinct zones within the Lower Goru B and C Sands levels in both wells. In the C interval, hydrocarbon saturation (Sh) falls within the range of 71% to 86%, while in the B interval, Sh ranges from 30% to 50%. These findings suggest that the C interval possesses a greater potential for hydrocarbon accumulation.
3. Seismic inversion analyzed impedance changes in C and B intervals of the Lower Goru Formation. It identified a significant impedance drop at Sawan 01 and Sawan 07 along the C sand channel, suggesting possible hydrocarbon accumulation. In contrast, the B sand channel showed lower impedance only at Sawan 01, indicating higher hydrocarbon potential in the C interval.
4. Machine learning analysis, categorizing them into three distinct lithological packages: sand, shale, and tight sand.
5. Machine learning was applied in sequential steps. In the first step, the identified layer boundaries were utilized to compute the volume of shale from the gamma ray log, and a block averaging technique was applied within these boundaries.

Conflict of Interest

The authors showed no conflict of interest.

Funding

The authors did not mention any funding for this research.

References

Bäckstrand, K., Zelli, F., & Schleifer, P. (2022). Legitimacy and accountability in polycentric climate governance. *Nature Reviews Earth & Environment, 3*(6), 378–390. https://doi.org/10.1038/s43017-022-00291-6

Biermann, F., Abbott, K., Andresen, S., Bäckstrand, K., Bernstein, S., Betsill, M. M., Bulkeley, H., Cashore, B., Clapp, J., Folke, C., Gupta, A., Gupta, J., Haas, P. M., Jordan, A., Kanie, N., Kluvánková-Oravská, T., Lebel, L., Liverman, D., Meadowcroft, J., & Zondervan, R. (2012). Transforming governance and institutions for global sustainability: Key insights from the Earth System Governance Project. *Current Opinion in Environmental Sustainability, 4*(1), 51–60. https://doi.org/10.1016/j.cosust.2012.01.014

Biermann, F., Hickmann, T., Sénit, C. A., Beisheim, M., Bernstein, S., Chasek, P., Grob, L., Kim, R. E., Kotzé, L. J., Nilsson, M., Ordóñez Llanos, A., Okereke, C., Pradhan, P., Raven, R., Sun, Y., & Vijge, M. J. (2022). Scientific evidence on the political impact of the Sustainable Development Goals. *Nature Sustainability, 5*(9), 795–800. https://doi.org/10.1038/s41893-022-00909-5

Biermann, F., Kanie, N., & Kim, R. E. (2017). Global governance by goal-setting: The novel approach of the Sustainable Development Goals. *Current Opinion in Environmental Sustainability, 26–27*, 26–31. https://doi.org/10.1016/j.cosust.2017.01.010

Bowen, K. J., Cradock-Henry, N. A., Koch, F., Patterson, J., Häyhä, T., Vogt, J., & Barbi, F. (2017). Implementing the Sustainable Development Goals: Towards addressing three key governance challenges—Collective action, trade-offs, and accountability. *Current Opinion in Environmental Sustainability*, *26–27*, 90–96. https://doi.org/10.1016/j.cosust.2017.05.002

Bulkeley, H., & Mol, A. P. J. (2003). Participation and environmental governance: Consensus, ambivalence and debate. *Environmental Values, 12*(2), 143–154. https://doi.org/10.3197/096327103129341261

Folke, C., Polasky, S., Rockström, J., Galaz, V., Westley, F., Lamont, M., Scheffer, M., Österblom, H., Carpenter, S. R., Chapin, F. S., Seto, K. C., & Walker, B. (2021). Our future in the Anthropocene biosphere. *Ambio, 50*(4), 834–869. https://doi.org/10.1007/s13280-021-01544-8

Gupta, J. (2016). Climate change governance: History, future, and triple-loop learning? *WIREs Climate Change*, *7*(2), 192–210. https://doi.org/10.1002/wcc.388

Gupta, J., & Sanchez, N. (2012). Global green governance: Embedding the green economy in a global green and equitable rule of law polity. *Review of European Community & International Environmental Law*, *21*(1), 12–22. https://doi.org/10.1111/j.1467-9388.2012.00739.x

Gupta, J., Pahl-Wostl, C., & Zondervan, R. (2023). Strengthening institutional resilience for climate adaptation and sustainable development. *Current Opinion in Environmental Sustainability*, *62*. https://doi.org/10.1016/j.cosust.2023.101281

Hickmann, T., Biermann, F., Sénit, C. A., Beisheim, M., Bernstein, S., Chasek, P., Grob, L., Kim, R. E., Kotzé, L. J., Nilsson, M., Ordóñez Llanos, A., Okereke, C., Pradhan, P., Raven, R., Sun, Y., & Vijge, M. J. (2024). Global governance and the Sustainable Development Goals: Progress and future directions. *Nature Sustainability*. https://doi.org/10.1038/s41893-024-01329-5

Intergovernmental Panel on Climate Change. (2023). *Climate Change 2023: Synthesis Report*. https://www.ipcc.ch/report/ar6/syr/

International Energy Agency. (2023). *World Energy Outlook 2023*. https://www.iea.org/reports/world-energy-outlook-2023

Jordan, A. J., Huitema, D., van Asselt, H., Rayner, T., & Berkhout, F. (2023). Governing climate change: Polycentricity in action. *Annual Review of Environment and Resources*, *48*, 131–156. https://doi.org/10.1146/annurev-environ-112321-095825

Jordan, A., Huitema, D., van Asselt, H., Rayner, T., & Berkhout, F. (2018). *Governing climate change: Polycentricity in action?* Cambridge University Press. https://doi.org/10.1017/9781108284646

Newig, J., & Fritsch, O. (2023). Environmental governance and policy implementation: Recent advances and future directions. *Environmental Policy and Governance*, *33*(2), 81–95. https://doi.org/10.1002/eet.2019

Organisation for Economic Co-operation and Development. (2023). *Climate action monitor 2023*. https://www.oecd.org/climate-change/

Pahl-Wostl, C. (2009). A conceptual framework for analysing adaptive capacity and multi-level learning processes in resource governance regimes. *Global Environmental Change*, *19*(3), 354–365. https://doi.org/10.1016/j.gloenvcha.2009.06.001

Sachs, J. D., Lafortune, G., Fuller, G., & Drumm, E. (2024). *Sustainable Development Report 2024*. Sustainable Development Solutions Network. https://doi.org/10.25546/108572

Stevenson, H., & Dryzek, J. S. (2014). *Democratizing global climate governance.* Cambridge University Press. https://doi.org/10.1017/CBO9781139208628

United Nations Development Programme. (2024). *Human Development Report 2023/2024: Breaking the gridlock—Reimagining cooperation in a polarized world*. https://hdr.undp.org/

United Nations Environment Programme. (2024). *Emissions Gap Report 2024*. https://www.unep.org/resources/emissions-gap-report

United Nations. (2023). *The Sustainable Development Goals Report 2023: Special edition*. https://unstats.un.org/sdgs/report/2023/

Vinuesa, R., Azizpour, H., Leite, I., Balaam, M., Dignum, V., Domisch, S., Felländer, A., Langhans, S. D., Tegmark, M., & Nerini, F. F. (2020). The role of artificial intelligence in achieving the Sustainable Development Goals. *Nature Communications, 11*, Article 233. https://doi.org/10.1038/s41467-019-14108-y

World Bank. (2024). *State and trends of carbon pricing 2024*. https://openknowledge.worldbank.org/

Young, O. R. (2017). Governing complex systems: Social capital for the Anthropocene. *MIT Press.* https://doi.org/10.7551/mitpress/9780262036047.001.0001.